J. Fluid Mech. (1995), *vol.* 304, *pp.* 343–372

Experiments on subharmonic resonance in a shear layer

By HYDER S. HUSAIN AND FAZLE HUSSAIN

Department of Mechanical Engineering, University of Houston, Houston, TX 77204-4792, USA

(Received 20 February 1995 and in revised form 21 July 1995)

The subharmonic resonance phenomenon is studied using hot-wire measurements and flow visualization in an initially laminar shear layer forced with two-frequencies for various choices of the fundamental frequency f and its subharmonic $f/2$ with controlled initial phase difference ϕ_{in} between them. We explore the effects of the controlling parameters, namely: (i) forcing frequencies and their initial amplitudes, (ii) initial phase difference ϕ_{in}, and (iii) detuning (i.e. when the second forcing frequency is slightly different from $f/2$). While several of our experimental observations support predictions based on weakly nonlinear theory, others do not. We explain our data in terms of vortex dynamics concepts.

1. Introduction

The initiation, growth, interaction, breakdown, and regeneration of coherent structures are manifestations of a hierarchy of instabilities in turbulent shear flows. The coherent structure dynamics in transitional free shear flows are strongly dependent on the initial shear layer instability which, in turn, depends on initial flow states and perturbation characteristics.

Subharmonic resonance is a result of the nonlinear interaction between a wave of frequency f and its subharmonic $f/2$, producing an $f/2$ component which, depending on its phase, is capable of reinforcing the subharmonic (hence the term 'resonance'). The growth of the subharmonic is a key feature in mixing-layer dynamics because it leads to vortex pairing, which has important roles in technological applications. The presence of a subharmonic component as well as vortex pairing in a shear layer has been known for some time (e.g. Anderson 1955; Sato 1959; Bradshaw 1966; Browand 1966; Ho & Huang 1982); here we report new results documenting the phenomenon and explain them, primarily in terms of vortex dynamics.

In addition to obtaining a much needed basic understanding, a study of subharmonic resonance is important to enable turbulence management – enhancement or suppression – in mixing layers by manipulating the initial conditions. Turbulence management can contribute to the enhancement of large-scale engulfment, mixing, heat transfer and chemical reaction (including combustion), and reduction of drag and aerodynamic noise (Laufer 1974; Bridges & Hussain 1987). This management may be achieved in a jet or a single-stream mixing layer by using control parameters such as $St_{\theta_e}(\equiv f\theta_e/U_e)$, $a'_f(\equiv u'_{ef}/U_e)$, $a'_{f/2}(\equiv u'_{ef/2}/U_e)$, and ϕ_{in} (where f is the fundamental excitation frequency, θ_e is the exit momentum thickness, U_e is the free-stream velocity, u'_{ef} and $u'_{ef/2}$ are the initial r.m.s. longitudinal velocity perturbation amplitudes of the f and $f/2$ components, and ϕ_{in} is the initial phase difference between f and $f/2$). In this

paper, ϕ always refers to the $f-f/2$ phase *difference* (as defined in equation (2.1)) with spatial variations indicated by the subscript.

Initial instability. An initially laminar shear layer's sensitivity to disturbances has been accurately predicted using linear instability analysis (Michalke 1965) and verified experimentally (Freymuth 1966). Employing a composite expansion technique that accounts for both shear-layer spreading and critical-layer nonlinearities, Goldstein & Leib (1988) and Hultgren (1992) predicted the growth rate, saturation amplitude, and rollup of a fundamental wave and found good agreement with experimental results of Freymuth (1966). The amplification rate is highest at $St_{\theta_e} \approx 0.017$; thus, one would expect an unforced shear layer to roll up at this frequency. However, experimental studies by Zaman & Hussain (1980) revealed that an unexcited shear layer rolls up into discrete vortical structures at $St_{\theta_e} \approx 0.012$ and not at $St_{\theta_e} \approx 0.017$. (We refer to $St_{\theta_e} \approx 0.012$ as the 'natural instability frequency'.) Data also show that the maximum amplification (i.e. maximum saturation amplitude) occurs at $St_{\theta_e} \approx 0.012$ while excitation at $St_{\theta_e} \approx 0.017$ produces the maximum amplification rate, but saturation to a lower level. Saturation to a lower level and suppression of pairing are the causes of turbulence suppression observed by Zaman & Hussain (1981). Hussain (1986) argued that this anomaly in the vortex rollup frequency is a consequence of feedback being strongest at $St_{\theta_e} \approx 0.012$ (see §3.2.3).

We first examine the current theoretical, numerical, and experimental knowledge about subharmonic resonance and pairing, focusing on their limitations and the need for a comprehensive experimental study such as ours.

1.1. *Subharmonic resonance and vortex pairing*

Theory. The instability mechanism by which a subharmonic perturbation is amplified in a shear layer was first analysed by Kelly (1967) using a weakly nonlinear temporal theory for a parallel flow. The theory predicts that the growth of such perturbations is most pronounced when the fundamental amplitude is neutral and the perturbation frequency is half the fundamental. Pierrehumbert & Widnall (1982) performed a similar analysis but used the Stuart solution (Stuart 1967) as the steady basic state and treated its linear stability as a two-dimensional eigenvalue problem. Their results are in close agreement with those of Kelly.

Monkewitz (1988) extended Kelly's (1967) weakly nonlinear analysis to spatially growing waves in a parallel mixing layer with a hyperbolic-tangent profile. He addressed several aspects of subharmonic resonance, including: (i) the dependence of the subharmonic growth on ϕ_{xf} (phase difference at the fundamental saturation location x_f), (ii) the existence of a critical fundamental amplitude for resonant subharmonic growth, and (iii) the effects of detuning. More recently, Cheng & Chang (1992) derived the onset criteria for subharmonic instabilities accounting for $O(3)$ terms in the amplitude equation. (Note that Kelly 1967 and Monkewitz 1988 used terms up to $O(2)$.) In contrast to the $O(2)$ analysis, Cheng & Chang showed that a finite-amplitude wave is always unstable to disturbances with half its frequency if the subharmonic is linearly unstable. However, this higher-order theoretical analysis has contributed little to understanding of the flow.

Limitations of the theory. Pierrehumbert & Widnall (1981) and Mankbadi (1985) have explained rollup, pairing, and shredding in terms of energetics, but not the associated vortex dynamics. Laboratory (and most technological) flows do not satisfy the assumptions invoked in the theoretical analysis of Monkewitz (1988), namely, weak nonlinearity, slight flow divergence, and a neutral fundamental. Furthermore, the assumed constant profile is not consistent with his slightly non-parallel mean flow

approximation (Monkewitz 1988) and disallows the vortices from moving transversely (during actual pairing). As a result, this model cannot describe vortex pairing and is valid at most for a small region near x_f.

Numerical simulations. Riley & Metcalfe (1980) and Corcos & Sherman (1984) numerically studied subharmonic resonance for temporally growing mixing layers and found that the kinematics of the associated interactions depend critically on the initial phase difference between f and $f/2$. However, shear layers in virtually all technological flows are spatially evolving. There are clear differences in the pairing dynamics in these two flows, e.g. unequal induction by neighbouring structures on a pairing/paired vortex in a spatially developing flow (discussed in §3.1.2).

Experiments. Although the initial subharmonic amplitude measured by Zaman & Hussain (1980) and Drubka (1981) is in qualitative agreement with the theoretical prediction of Monkewitz (1988), their data lack details of subharmonic resonance. Additionally, the theoretically obtained critical fundamental amplitude (Monkewitz 1988) disagrees with Drubka's data.

Arbey & Ffowcs Williams' (1984) study of a circular jet (using two-frequency excitation at f and $f/2$) detected a dependence of the subharmonic growth on the phase difference ϕ in the excitation signal. Because they did not measure ϕ from velocity signals at the exit plane or at x_f, a direct comparison of their data with either theoretical results or the present experiments is not possible. Hajj, Miksad & Powers (1993) concluded that the maximum subharmonic growth occurs at a single phase, in contrast to Monkewitz's (1988) prediction of subharmonic enhancement over a wide range of ϕ_{xf}. This is not surprising because Hajj *et al.* investigated subharmonic resonance at four phases only. In a recent experiment in an axisymmetric jet, Paschereit, Wygnanski & Fiedler (1995) also observed dependence of the subharmonic growth on the phase angle.

1.2. *Motivation and goals*

Since subharmonic resonance typically leads to vortex pairing, vortex dynamics and classical instability analysis of interacting waves should complement each other to provide a better understanding of the phenomenon. The initial disturbance waves (fundamental and subharmonic) govern the strengths of vortices at rollup, their streamwise spacing, and their transverse displacement, which subsequently control pairing dynamics. However, previous subharmonic resonance studies have not focused on the dynamics of interacting vortices.

One of our long-term goals is to model the pairing phenomenon and use the model for prediction and control. Based on a conceptual model of the flow physics, experiments can reveal the effects of control parameters, which can then be incorporated into low-dimensional mathematical models. Since subharmonic resonance and pairing have been found to be crucial elements of periodic and chaotic vortex dynamics in shear layers and jets (Narayanan & Hussain 1995; Broze & Hussain 1994), well-controlled subharmonic resonance experiments can provide a key input for such models.

The present study (employing controlled, two-frequency, phase-locked, and detuned excitation) examines the development of sideband frequencies and transition to turbulence of natural (unforced) or excited (with a single frequency) shear layers in addition to recommending methods for turbulence and mixing control. This study has the following objectives: (i) to understand the flow physics associated with subharmonic resonance and interpret the theoretical predictions in terms of vortex dynamics and (ii) to achieve turbulence control by exploiting the dependence of subharmonic resonance on control parameters. The experimental apparatus and procedure are described in §2.

The results are discussed in §3, which include the effects of ϕ_{in}, f, and detuning. Concluding remarks are presented in §4.

2. Experimental apparatus and procedure

2.1. *Air jet facility*

Hot-wire measurements were made in the shear layer of a 27 cm diameter jet (figure 1*a*). A centrifugal blower with a Poly Spede motor controller permitted speed control within $\pm 0.1\%$ of the full range of 2500 r.p.m. Room air enters the blower through a 1 m × 1 m filter box fitted with multistage fibreglass filters. The inlet section of the blower has a honeycomb (0.63 cm cell and 5.4 cm deep) to eliminate large intake swirls. The flow from the blower passes through a silencer (consisting of Helmholtz and quarter-wave resonators) and a three-stage square diffuser (each 1.5 m long). There is a 24-mesh screen between each stage. The diffuser section is followed by a 3.6 m long settling chamber fitted with 12 screens and a honeycomb. The 8:1 nozzle has a cubic profile with a 13 cm straight section at the exit.

The shear layer was excited by a speaker through a narrow uniform slit (0.5 mm) along the nozzle exit perimeter. A large speaker in the speaker box produced pressure pulses which were transmitted to the excitation box through four 28.5 mm diameter tubes of equal lengths, assuring identical phases of pressure pulses transmitted from the speaker box to the shear layer excitation slit. The speaker box is enclosed in a steel box with foam padding so that pressure can only be transmitted through the tubes.

An excitation signal, consisting of two harmonically related frequencies, was produced by a phase-locked generator to drive the speaker. The velocity perturbation produced at the shear-layer origin was of the following form with negligible higher-harmonic contents:

$$u = a_f \cos(2\pi ft) + a_{f/2} \cos(\pi ft + \phi_{in}). \tag{2.1}$$

Velocity data were obtained by a linearized constant-temperature hot-wire anemometer (DISA). A special long-prong probe (TSI-1210C) was placed at an angle such that the probe stem remained outside the flow, producing no probe-induced shear-layer tones (Hussain & Zaman 1978). Phase angles were measured by a digital signal analyser (Ono-Sokki CF-920). A laboratory minicomputer (HP 2100) was used for traverse control, data acquisition, and on- and off-line data processing.

2.2. *Initial boundary-layer characteristics*

The exit-plane boundary-layer characteristics (longitudinal mean and r.m.s. velocity distributions) were measured at several exit velocities to find the velocity range over which the boundary layer remained laminar. As examples, exit boundary-layer profiles at three jet velocities ($U_e = 12.2$, 15.2 and 18.3 m s^{-1}) are shown in figure 1(*b*). Although the measured mean velocity data agree well with the Blasius profile (shown by the solid line) and have shape factors close to 2.59, profiles of turbulence intensity indicate that the boundary layer is transitional for $U_e > 17$ m s^{-1}. This reinforces our claim that the mean velocity profile alone cannot indicate whether or not a boundary layer is laminar (Hussain 1983). In all cases, the longitudinal fluctuating velocity profiles show peaks at $y \sim \delta^*$, as explained by Hussain & Clark (1977), and decrease monotonically to the free-stream value of about $u_e'/U_e = 0.1\%$. Note that the free-stream turbulence of 0.1% is almost entirely due to room acoustic modes in the 6–10 Hz range, quite distinct from the excited fundamental (200–500 Hz) or the subharmonic.

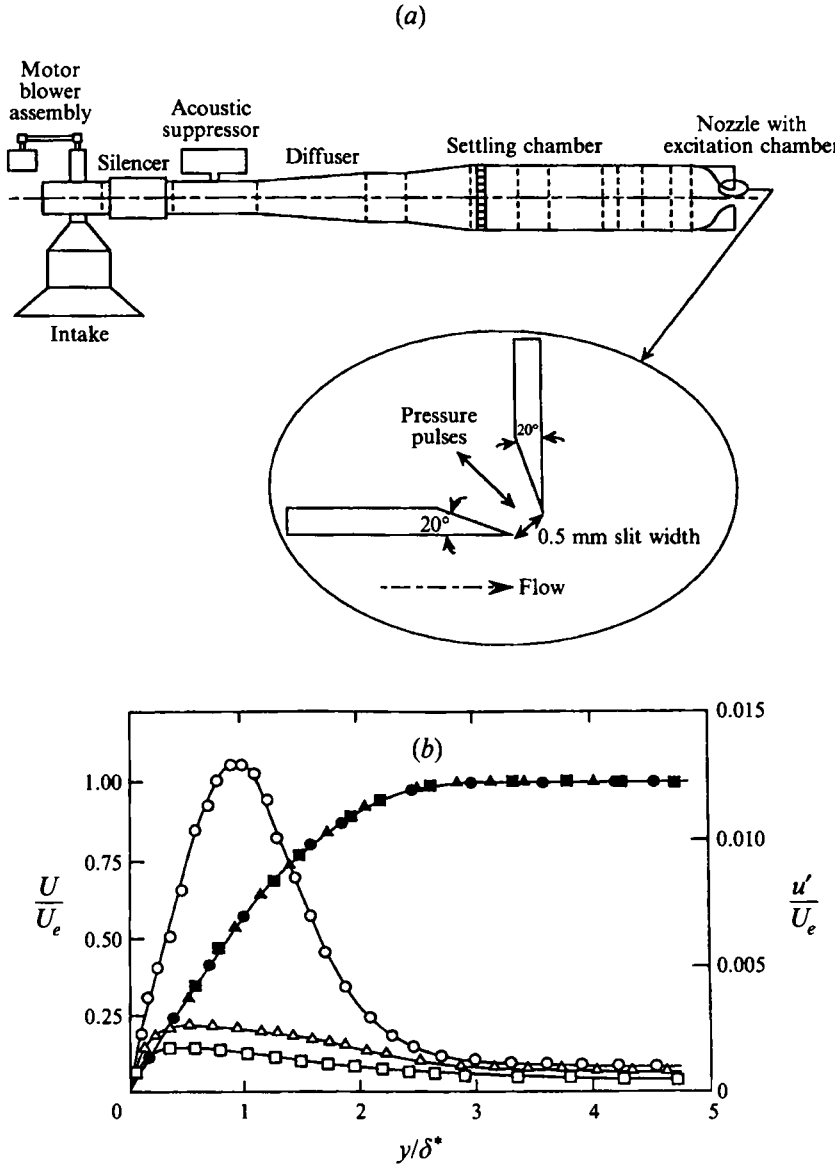

FIGURE 1. (*a*) Schematic of the air jet facility with a lip excitation system. (*b*) Boundary-layer characteristics in the air jet; profiles of mean (solid symbols) and r.m.s. intensity (open symbols) of u at three jet velocities: □, 12.2 m s^{-1}; △, 15.2 m s^{-1}; ○, 18.3 m s^{-1}. The solid line through the mean velocity data represents the Blasius profile. The high turbulence intensity for $U_e \approx 18.3$ m s^{-1} indicates a transitional boundary layer.

To avoid transitional exit boundary layers, the present studies were performed at exit velocities below 15.2 m s^{-1}. Since the shear-layer excitation system has discrete resonance frequencies, both velocity and frequency were adjusted to obtain the desired St_{θ_e} values. Variation of the exit momentum thickness θ_e/D with Reynolds number Re_D ($\equiv U_e D/\nu$) was measured. Within the velocity range $10.7 < U_e < 18.3$ m s^{-1}, θ_e/D has the expected power-law variation with Re_D. A least-squares fit of the data has the form $\theta_e/D = 2.4 \times 10^{-5} + 0.755 Re_D^{-0.5}$. Using this expression and the available resonance frequencies of the excitation system, U_e was selected to achieve a desired St_{θ_e} value.

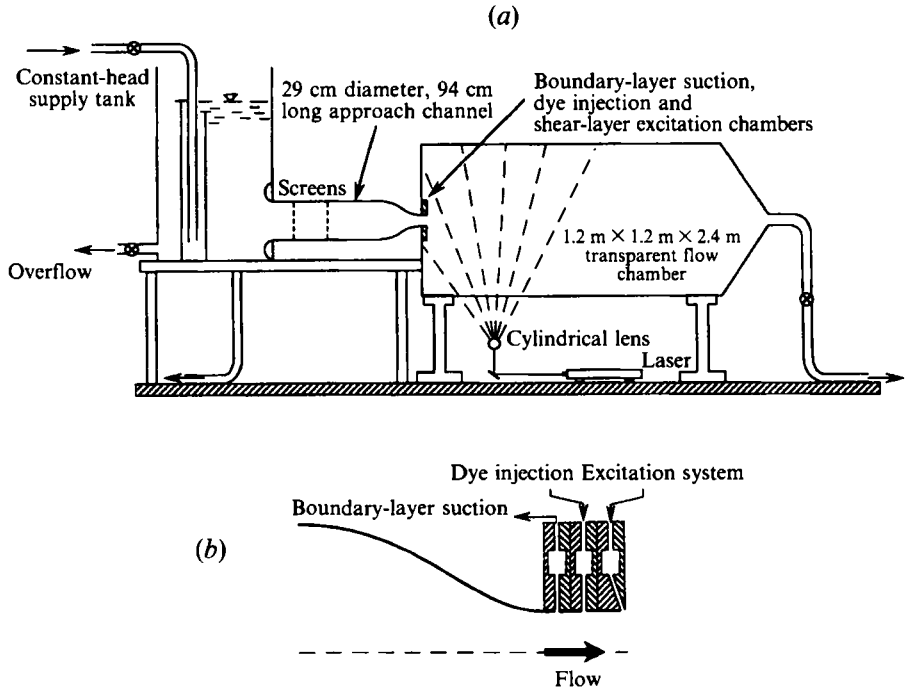

FIGURE 2. Schematics of: (*a*) water jet facility with flow visualization equipment; (*b*) dye injection and excitation system.

Note that within the operating U_e range, θ_e is orders of magnitude smaller than the diameter D (e.g. $D/\theta_e \approx 670$ at $U_e = 14.5$ m s^{-1}), indicating that the effect of nozzle exit curvature on the initial evolution of the shear layer is negligible.

2.3. *Water jet*

Flow visualization was performed in a submerged water jet facility (figure 2*a*). A constant-head supply tank upstream of the contraction nozzle maintained a prescribed flow rate. Two 28 mesh screens were placed in the settling chamber to minimize upstream disturbances. A 10 cm circular nozzle with a 9:1 contraction ratio was used for this study.

The shear layer was excited at the nozzle exit plane through a 0.5 mm slit using an electromagnetic shaker, actuating a piston in a cylinder containing water. The cylinder outlet was connected to the outer perimeter of the shear layer excitation chamber through four tubes of equal lengths. Thus, periodic perturbations were transmitted through water from the cylinder to the excitation chamber and finally to the nozzle exit boundary layer (figure 2*b*). The Reynolds numbers Re_D based on the jet diameter D for the air and water jets are different: for the air jet, $Re_D \sim 230000$, while for the water jet, $Re_D \sim 50000$. However, for our study, Re_D is not an important parameter since the near-exit flow is quasi-two-dimensional with a large D/θ_e ($\sim 10^3$).

To visualize the flow, a low-concentration fluorescent dye (Uranamine) was supplied through a second narrow slit along the nozzle perimeter about 1 cm upstream of the exit plane. The height of the dye reservoir was adjusted such that the dye seeped into the boundary layer without introducing any perceptible disturbances. A cylindrical lens flared a 12 W Ar–ion laser beam into a thin sheet to illuminate the plane of interest in the flow field.

Video recorded images, digitized by a Colorado Video Model 274 frame grabber, were enhanced using an International Imaging System (IIS 600) image processor; and the intensity contours were computed using a Masscomp 5500 computer. The flow visualization data are presented in the form of isointensity contours of light emitted by the fluorescent dye.

3. Results and discussion

We first address the role of ϕ_{in} in modifying vortex configurations leading to subharmonic enhancement or attenuation. Using low-level, two-frequency, phase-locked excitation, we examine the St_{θ_e} range over which vortex pairing can be affected. Then, results of controlled detuned excitation are compared with theoretical predictions. Furthermore, these results are used to analyse the evolution of natural (unforced) shear layers.

3.1. *The role of phase angle in subharmonic growth*

Because of dispersion, the exit phase difference ϕ_{in} evolves to ϕ_{xf} at x_f where resonance begins. Theory (Monkewitz 1988) predicts that the subharmonic is attenuated at a critical value of ϕ_{xf} but enhanced over a wide range of ϕ_{xf}. This will be verified in this subsection and in §3.3. The value of ϕ_{in} required for maximum enhancement or suppression is not fixed and depends on St_{θ_e} as well as a'_f, as the phase speed and x_f vary with St_{θ_e}, and x_f varies with a'_f. We have determined the values of ϕ_{in} that produce enhancement and attenuation of the subharmonic for various St_{θ_e} and excitation levels. In the following, we show results for excitation only at the natural instability frequency and its subharmonic, i.e. $St_{\theta_e} = 0.012$ and 0.006 with $a'_f = a'_{f/2} = 0.1\,\%$.

The dependence of the subharmonic amplitude $u'_{f/2}$ on ϕ_{in} was examined at a number of streamwise stations. Note that the range $0 \leqslant \phi_{in} \leqslant \pi$ covers one period of the fundamental (equation (2.1)). At each x station, measurements were made at the transverse location of peak $u'_{f/2}$ (for each ϕ_{in}). The variations of u'_f and $u'_{f/2}$ with ϕ_{in} are shown in figure 3(*a–c*) for $x/\theta_e = 30$ (upstream of x_f), 80 (downstream of x_f) and 140 (downstream of the subharmonic saturation location x_s). The initial phases ϕ_{in} which correspond to maximum enhancement and attenuation of the subharmonic are denoted by ϕ_{en} and ϕ_{at} respectively.

As expected, at $x/\theta_e = 30$, u'_f and $u'_{f/2}$ are almost constant for all ϕ_{in} (figure 3*a*) since u'_f and $u'_{f/2}$ grow independently upstream of x_f. However, downstream of x_f, $u'_{f/2}$ shows significant variations with ϕ_{in}. At $x/\theta_e = 80$, we find $\phi_{en} \sim 150°$ and $\phi_{at} \cong 72°$ (figure 3*b*). The subharmonic amplitude $u'_{f/2}$ shows a cusp-like behaviour at ϕ_{at}. At the third location (i.e. $x/\theta_e \approx 140$; figure 3*c*), $u'_{f/2}$ decreases sharply at ϕ_{at}, but the corresponding value of $u'_{f/2}$ is higher than it is at $x/\theta_e = 80$. This higher value is due to intermittent pairings because the configuration of rolled-up vortices for ϕ_{at} (discussed later in this section) is unstable. At $x/\theta_e = 140$, $u'_{f/2}$ is smaller at the enhancement phase ($\phi_{in} \approx 140°$) than at $\phi_{in} \approx 30°$ and 90°, because $u'_{f/2}$ has saturated in the former case at an earlier location ($x_s \approx 124\theta_e$). However, pairing is delayed for ϕ_{in} ($\approx 30°$, 90°) near ϕ_{at}. Thus, at $x/\theta_e \approx 140$ the $u'_{f/2}$ values are higher for these phases than for those near ϕ_{en} ($\phi_{in} \approx 140°$), since decay following saturation has not yet begun.

Experiments at higher excitation levels (e.g. $a'_f = a'_{f/2} = 1\,\%$) produce results (not shown) similar to figure 3, except that $\phi_{en} \sim 120°$ and $\phi_{at} \approx 27°$. Since higher a'_f moves x_f upstream but ϕ_{xf} remains constant for enhanced ($\approx \pi/2$) or suppressed (≈ 0) pairing (see §3.1.1), the flow must evolve from a different ϕ_{in} in order to reach the necessary phase at x_f. The fundamental saturates at $x_f \approx 60\theta_e$ for 0.1 % excitation, but at

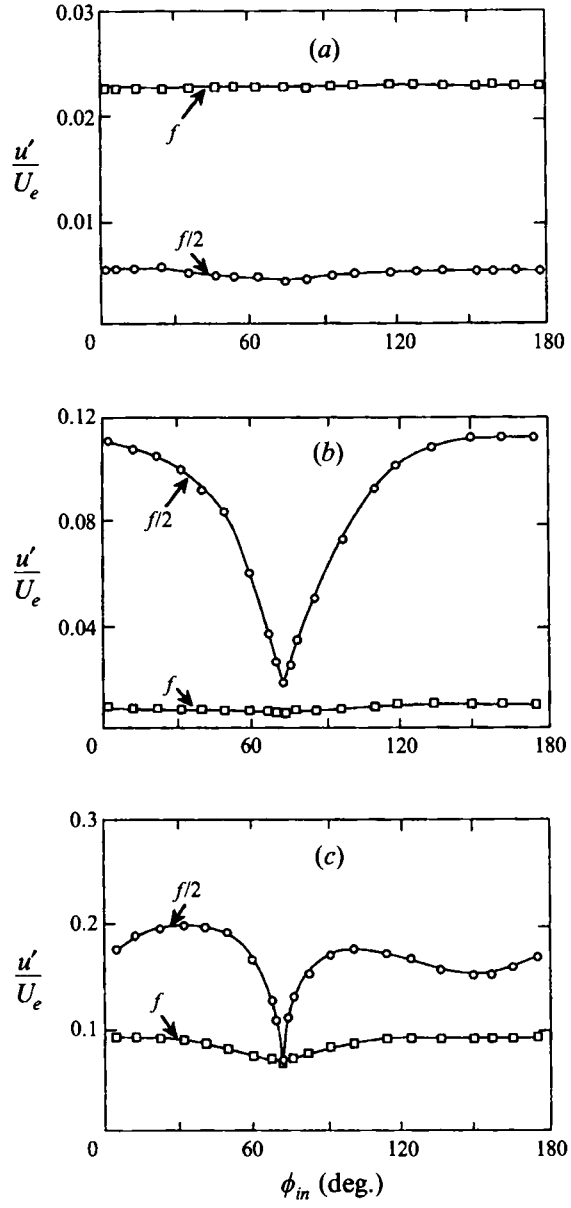

FIGURE 3. Dependence of u'_f and $u'_{f/2}$ on ϕ_{in}: (*a*) $x/\theta_e = 30$; (*b*) $x/\theta_e = 80$; (*c*) $x/\theta_e = 140$. $St_{\theta_e} = 0.012$; $a'_f = a'_{f/2} = 0.1\,\%$. □, u'_f; ○, $u'_{f/2}$. $u'_{f/2}$ is strongly attenuated at a critical value of $\phi_{in} \approx 72°$, while $u'_{f/2}$ is enhanced over a wide range of ϕ_{in}. Note that u'_f shows very little variation with ϕ_{in}.

$x_f \approx 40\theta_e$ for 1 %. Thus, for a fixed St_{θ_e}, variation in ϕ_{en} or ϕ_{at} with a'_f is due to the changes in x_f.

The dependence of the modified subharmonic growth rate near x_f on phase difference ϕ_{in} is a crucial element of the periodic and chaotic dynamics found in jets (Broze & Hussain 1994) and shear layers (Narayanan & Hussain 1995). In these experiments, f was forced and $f/2$ perturbations came from pairing feedback. They hypothesized that if a'_f is large enough, a modified $f/2$ growth rate will occur which leads to phase-locked $f/2$ feedback (hence periodic pairing). Lower a'_f will not permit

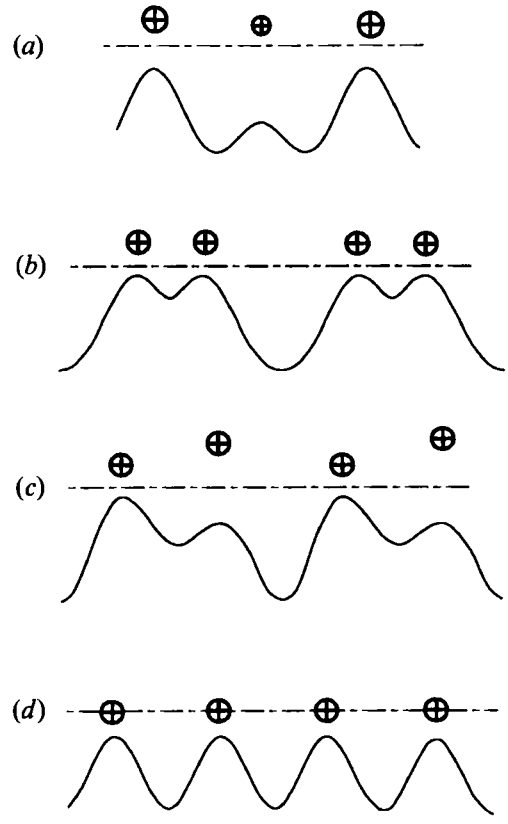

FIGURE 4. Possible vortex configurations which result in the enhancement and attenuation of the subharmonic component. (*a*) Equally spaced vortices, but with alternating high and low strengths; (*b*) equally strong vortices with alternating large and small spacing; (*c*) equally strong and equally spaced, but staggered transversely; (*d*) equally strong and equally spaced vortices. ⊕ indicates vortex centre.

phase locking, and ϕ_{in} will wander through all phases including enhancement and attenuation phases.

Clearly, ϕ_{xf} controls pairing enhancement or suppression. As we explain below (§3.1.1), it does so by controlling the configuration of vortices at rollup and, hence, their subsequent interactions. To make this connection clear, we examine the vortex configurations (and their induced motions) at different ϕ_{xf}. For this purpose, we consider the $\tilde{u}$-signal on the high-speed side of the shear layer because single hot-wire measurements there provide clean signals without significant measurement inaccuracies, including effects of flow reversal on the zero-speed side.

3.1.1. *Vortex configurations and their induced velocity fields*

After the shear-layer vortices roll up, a subharmonic component appears in the $\tilde{u}$-signal for any one (or a combination) of the following vortex configurations shown in figure 4(*a–c*): (*a*) equally spaced vortices advecting along a straight line, but with alternate high and low strengths; (*b*) equal-strength vortices with alternating larger and smaller spacings; or (*c*) equally spaced vortices of equal strength, but alternately staggered in the transverse direction. The subharmonic component in the velocity signal will be absent only when equally strong and equally spaced vortices advect along a straight line (figure 4*d*).

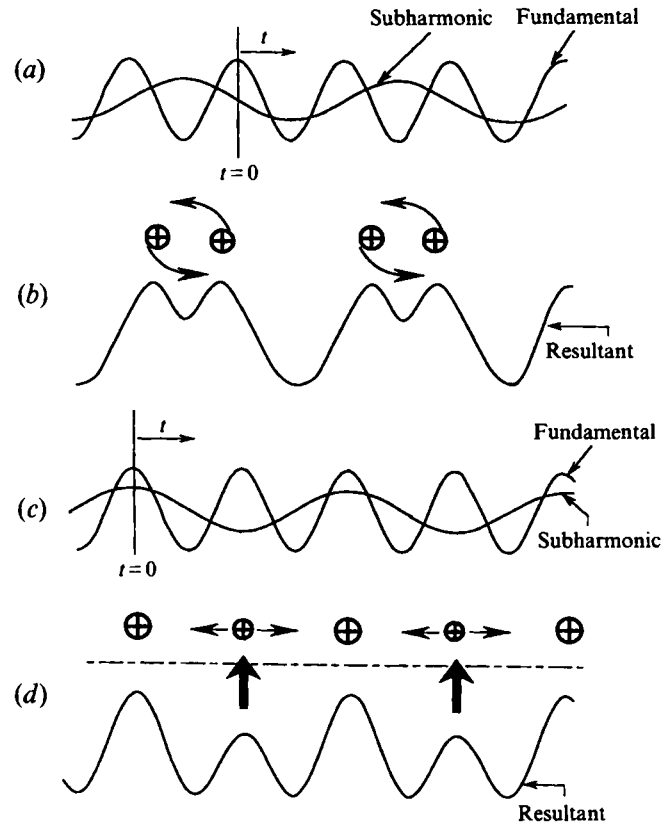

FIGURE 5. Schematics showing streamwise velocity fluctuations on the high-speed side of a shear layer and the corresponding vortex configurations for: (a, b) ϕ_{en}; (c, d) ϕ_{at}. $\oplus$ indicates vortex centre.

Consider vortex configurations at x_f which cause subsequent subharmonic enhancement or attenuation. First, note that the exit velocity perturbation controls the vortex configuration, and vortex centres are formed at the location where the transverse gradient of u (i.e. ω_z) is maximum. Secondly, note that the peak in u lies transversely away from the vortex centre towards the high-speed side where measurements are made. For $\phi_{xf} = \pi/2$, the peaks of the subharmonic perturbation lie between adjacent peaks of the fundamental perturbation (figure 5*a*), causing peaks in the resultant perturbation to move closer (figure 5*b*); and hence vortices roll up alternately close to and farther from their neighbours. The two nearby vortices thus produced undergo pairing through mutual induction. On the other hand, for $\phi_{xf} = 0$, the resultant perturbation has alternately high and low peaks (figure 5*c*, *d*), presumably producing vortices which are equally spaced but alternating in strength. The mutual inductions on a particular vortex from its neighbouring upstream and downstream vortices are equal but in opposite directions. As a result, the vortices advect in a straight line, and hence pairing is suppressed.

In the following, we show three kinds of vortex interactions, namely (i) enhanced pairing, (ii) non-pairing advection of vortices and (iii) shredding, observed via flow visualization under excitation at the natural instability frequency (i.e. $St_{\theta_e} = 0.012$) and its subharmonic. Forcing levels a'_f and $a'_{f/2}$ were not measured in the flow visualization studies. The relative levels of these two were controlled in the driving signal of the

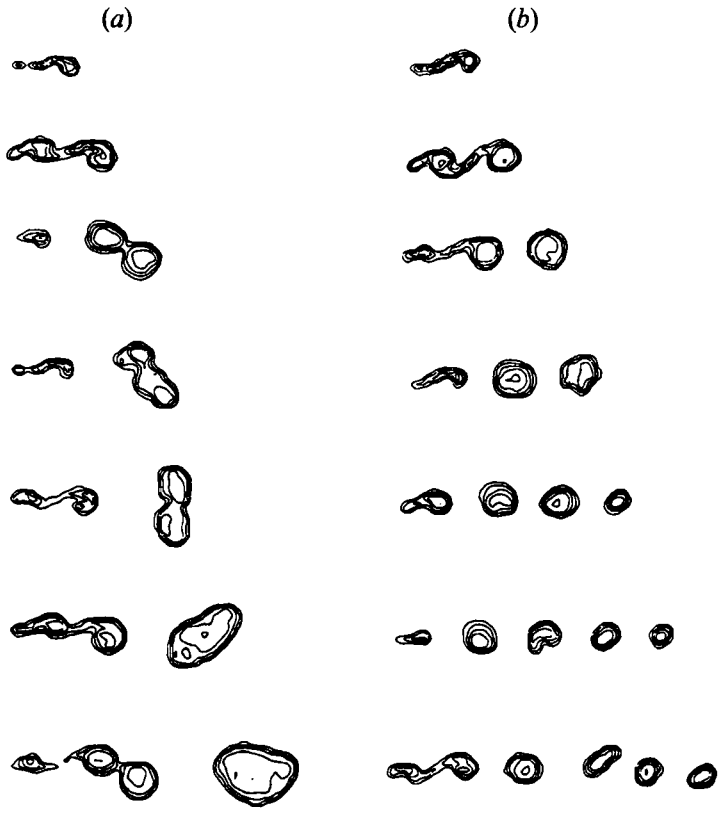

FIGURE 6. Isointensity contours of flow visualization pictures for low AR_{in}. (*a*) $\phi = \phi_{en}$, enhanced pairing (completed at frame 6); (*b*) $\phi = \phi_{at}$, suppression of pairing showing straight-line vortex configuration (see frames 4 to 7).

excitation device. Flow visualization data are presented in the form of isointensity contours of the fluorescent dye (figures 6 and 7).

3.1.2. *Enhanced pairing and advection of unpaired vortices*

When excited at ϕ_{en} with a low initial amplitude ratio AR_{in} ($\equiv a'_{f/2}/a'_f$), two vortices undergo pairing immediately after rollup (figure 6*a*). On the other hand, for ϕ_{at} at the same excitation levels, equally spaced vortices form and advect downstream along a virtually straight line (figure 6*b*). However, this straight-line configuration is unstable to small perturbations, and ambient disturbances cause the vortices (by altering the phase difference at the lip and circulation during rollup) to undergo pairing farther downstream (although once a pairing is initiated, pairing feedback may sustain subsequent pairings for some time.) By *ambient disturbances* we mean perturbations (e.g. noise from the blower, air-conditioning system, standing acoustic modes in the laboratory, or flow in the breakdown region and beyond) produced outside the domain of interest (i.e. from the exit plane to the end of the jet potential core).

Note that the vortex configurations in a spatially developing shear layer (figure 6*a*) are quite different from those in a temporally evolving shear layer. In the present case, the induction on a particular vortex (say the second vortex from left in the sixth panel of figure 6*a*) by the upstream single vortex and the downstream paired vortex are unequal.

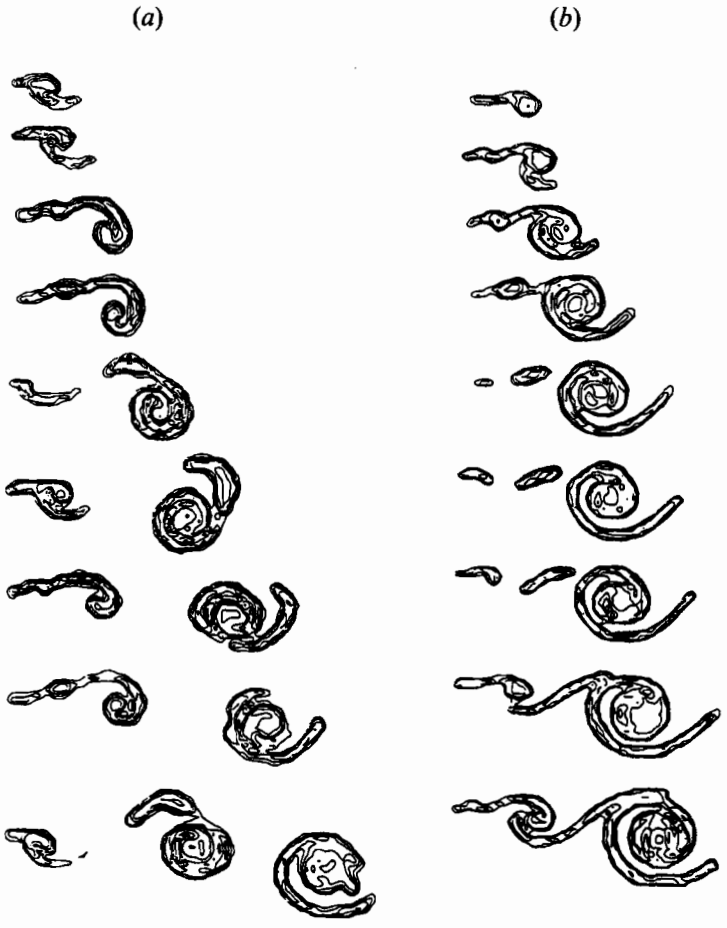

FIGURE 7. Isointensity contours of flow visualization pictures for high AR_{in}. (*a*) $\phi = \phi_{en}$; and (*b*) $\phi = \phi_{at}$. High AR_{in} produces smaller and larger vortices alternately. In (*a*), vortex interaction shows complete pairing (frame 6). In (*b*), shredding of the smaller vortex by its neighbouring vortices is evident in frames 5 to 9.

3.1.3. *Shredding*

Shredding refers to the situation when a weak vortex is at the saddle between two stronger vortices. The stronger vortices shear the weak one and pull it apart, each of the former capturing a part of the latter. We found significant shredding under strong subharmonic excitation (i.e. high AR_{in}) at ϕ_{at}, which produces equally spaced vortices with a weaker vortex at the location where the f and $f/2$ waves are out of phase (denoted by vertical arrows in figure 5*d*). Owing to the straining action of the two stronger vortices, vorticity from the weak vortex is transported to the neighbouring vortices (clearly visible in the flow visualization shown in figure 7*b*). Because the visualization experiments were for qualitative information, the excitation levels required for shredding before three-dimensional deformation were not recorded. A small deviation from ϕ_{at} inhibits shredding and initiates pairing (figure 7*a*).

AR_{in} is important in determining whether complete shredding or non-paired advection occurs. For excitation at ϕ_{at} with decreasing AR_{in}, the difference in strength between neighbouring vortices decreases. As a result, shredding progresses more slowly and thus takes place over a longer distance. However, in reality, three-dimensional

deformation of spanwise vortices (rolls), generation of longitudinal vortices (ribs), rib–roll interaction, and breakdown of rolls take place long before the completion of shredding.

In summary, we have identified initial phase angles that maximally enhance or suppress the subharmonic growth and explained the associated flow physics (e.g. pairing, non-pairing advection of vortices, and shredding) in terms of vortex dynamics.

3.2. *Effects of* St_{θ_e}

We observed that under low-amplitude ($a_f' \leqslant 0.1\,\%$), single-frequency excitation, periodic pairing occurs within a narrow band of St_{θ_e} (around 0.012). Is it possible to achieve periodic pairing over a wider range of St_{θ_e} values using low-amplitude, two-frequency excitation and a controlled ϕ_{in}? Because the growth rate depends on St_{θ_e}, the local amplitude ratio AR_{xf} ($\equiv u_{f/2}'/u_f'$ at x_f) will change with St_{θ_e} even for a fixed AR_{in}. As a result, relative vortex strengths and orientations will vary with St_{θ_e}. Thus, one would expect the details of vortex pairing to depend on St_{θ_e}. To study this dependence, we have examined the development of u_f' and $u_{f/2}'$ along the lip line for $0.006 \leqslant St_{\theta_e} \leqslant 0.024$ (figure 8*a–d*). Both a_f' and $a_{f/2}'$ were 0.1 %, and the excitation phase was ϕ_{en}.

3.2.1. *Fundamental*

By increasing St_{θ_e} up to 0.017, the fundamental growth rate increases, the saturation amplitude decreases, and x_f moves upstream (figure 8*a*, *b*). Further increases in St_{θ_e} cause a rapid decrease in the growth rate and the saturation amplitude. Excitation at $St_{\theta_e} = 0.024$ even leads to an initial decay of the fundamental up to $x/\theta_e \approx 6$, and the u_f' growth farther downstream appears to be due to generation of the first harmonic of the subharmonic. (Note that growth trends of the measured u_{2f}' when excited at $St_{\theta_e} = 0.012$ (not shown) match quite well with those of u_f' for $St_{\theta_e} = 0.024$ for $x/\theta_e \approx 25$–60.) Freymuth's (1966) experiments using single-frequency excitation at $a_f' = 0.3\,\%$ do not provide data near the exit plane for $x/\theta_e \leqslant 8$ for comparison. Figure 8(*e*) compares the growth rate data with those of Freymuth (1966). Results of the inviscid linear spatial stability analysis for two-dimensional parallel mixing layers by Monkewitz & Huerre (1982) for tanh velocity profiles ($R = 1$ and $R \ll 1$) and by Balsa (1987) for a piecewise linear velocity profile ($R = 0.5$) are also shown. (Here $R = (U_1 - U_2)/2\bar{U}$, and $\bar{U} = (U_1 + U_2)/2$ defined for two streams.) In figure 8(*e*), St_θ equals $f\theta/\bar{U}$, i.e. twice our parameter St_{θ_e} since $\bar{U} = U_e/2$. Unlike the growth rate characteristics for tanh-profiles, piecewise linear profiles show a rapid decrease in the growth rate for $St_\theta \geqslant 0.036$. Our data agree better with the spatial theory ($R = 1$) for $St_\theta \leqslant 0.036$ and show a rapid decrease in the growth rate for $St_\theta \geqslant 0.036$ following a trend similar to Balsa's results. In contrast, Freymuth's data are close to the results of Monkewitz & Huerre (1982) for $R \ll 1$, which is equivalent to the temporal formulation using a space–time transformation (Ho & Huerre 1984). The initial decay of u_f' at $St_\theta = 0.048$ in our experiment and the absence of any disturbances of the streaklines over a long distance in Freymuth's flow visualization at $St_\theta = 0.05$ (his figure 28) indicate that the instability range does not extend up to $St_\theta = 0.08$, as obtained by Monkewitz & Huerre (1982), but to a much lower value, $St_\theta \sim 0.046$.

An interesting aspect of the present experiment is that the growth rate data are in close agreement (up to $St_{\theta_e} \approx 0.017$) with the spatial analysis of Monkewitz & Huerre (1982), while Freymuth's data show lower growth rates. Note that the present experiments were performed using lip excitation, whereas Freymuth used bulk excitation of the jet. We performed experiments using bulk excitation and obtained

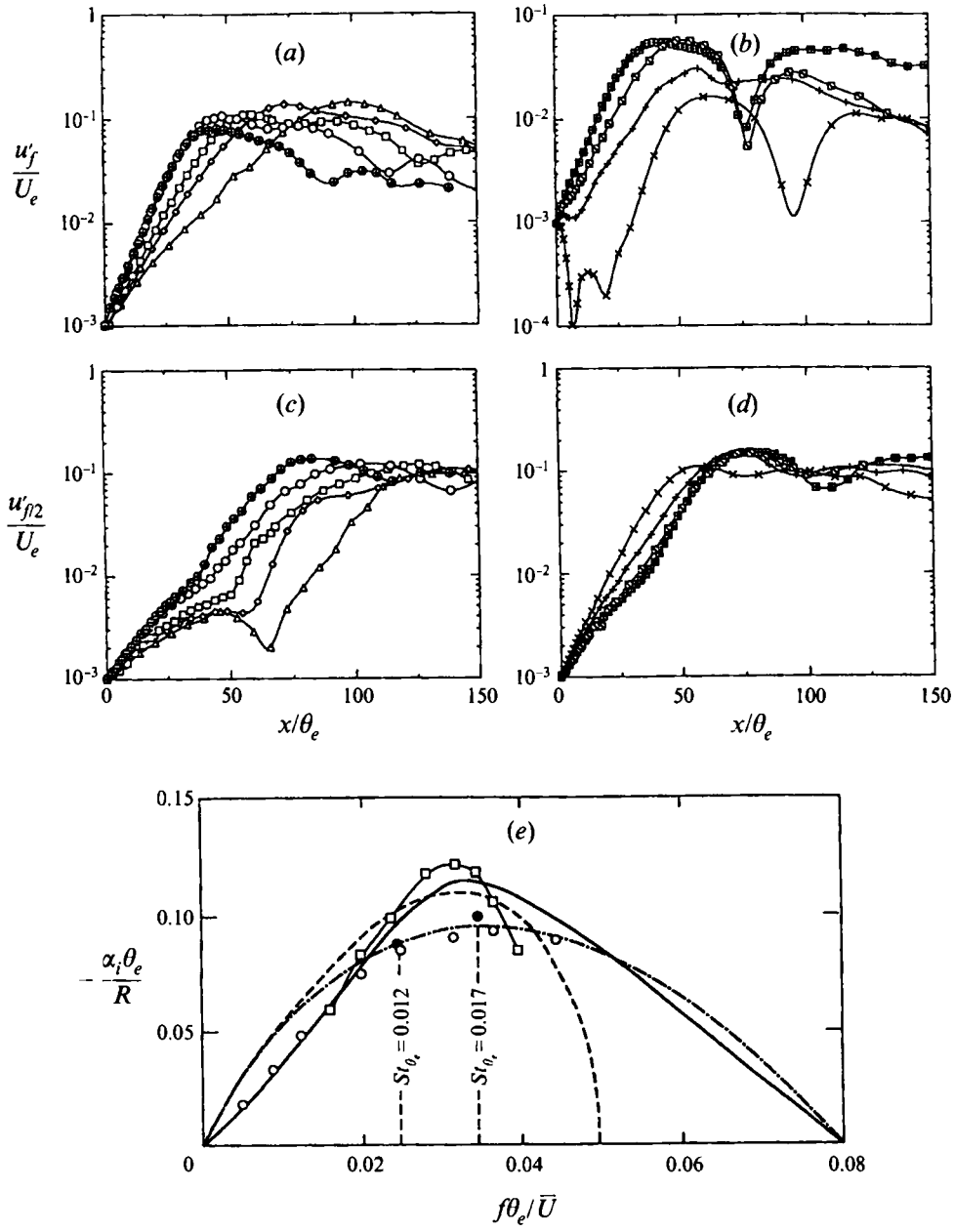

FIGURE 8. Growth trends of: (*a*, *b*) $u'_f(x)$ and (*c*, *d*) $u'_{f/2}(x)$ along the lip line for different St_{θ_e}: △, 0.008; ◇, 0.01; □, 0.012; ○, 0.014; ⊕, 0.016; ⊞, 0.017; ⧅, 0.018; +, 0.02; ×, 0.024. $a'_f = a'_{f/2} = 0.1\%$; $\phi = \phi_{ex}$. The subharmonic $u'_{f/2}$ undergoes a modified growth near the fundamental saturation location x_f, indicating resonant growth of the subharmonic. At a lower St_{θ_e} (≈ 0.008), $u'_{f/2}(x)$ shows a negative growth rate before it attains a strongly positive growth rate near x_f. (*e*) Spatial growth rates ($-\alpha_i\theta_e/R$) of the fundamental in the linear region. □, lip excitation and ●, bulk excitation (our data); ○, Freymuth's data (using bulk excitation). Note that lip excitation produces a higher growth rate than bulk excitation. Spatial theory: ——, $R = 1$; —— –, $R \ll 1$ (Monkewitz & Huerre 1982); – – –, $R = 0.5$ (Balsa 1987).

growth rates of $-\alpha_i \theta/R = 0.085$ and 0.1 at $St_\theta = 0.024$ and 0.034 (i.e. $St_{\theta_e} = 0.012$ and 0.017), respectively (shown by solid circles in figure 8*e*). These values are close to Freymuth's data and temporal results. This is presumably due to the fact that there exit-plane perturbation profiles are different for lip and bulk excitation. Lip excitation produces a highly localized perturbation. On the other hand, bulk excitation produces non-zero disturbance levels away from the shear layer.

3.2.2. *Subharmonic*

In figure 8(*c*, *d*), the subharmonic initially grows independently according to the linear instability theory; and its growth rate increases with St_{θ_e} (within our measured St_{θ_e} range) which is consistent with the theoretical predictions (figure 8*e*). However, as x_f is approached, the $u'_{f/2}$ growth rate first decreases for a short distance and then increases to a higher rate (than in the linear region), indicating resonant interaction. This decrease is quite prominent at low St_{θ_e} (e.g. $St_{\theta_e} \approx 0.008$–0.012) but gradually diminishes with increasing St_{θ_e}. In fact, the modification of the growth rate near x_f is negligible for $St_{\theta_e} = 0.018$–0.024.

Is the observed decrease in $u'_{f/2}$ growth rate an artifact of measurement location (along the lip line $y = 0$), as flow divergence may cause changes in $u'_{f/2}(y)$? Profiles at a few x stations indeed show shifts in the locations of $u'_{f/2}$ peaks. The streamwise evolution of $u'_{f/2}$ peaks at a low St_{θ_e} ($= 0.008$) is shown in figure 9(*a*). Although the $u'_{f/2}$ peak distribution does not decay near x_f, this does show an almost zero growth rate over short distance near x_f. This local arrest of the subharmonic growth is explained below in terms of vortex induction inferred from flow visualization and hot-wire data.

For a given St_{θ_e} AR_{xf} increases with AR_{in}, producing pairs of rolled-up vortices closer to each other. As an example, compare figures 6(*a*) and 7(*a*) (both at $St_{\theta_e} = 0.012$ and ϕ_{en}). A high AR_{xf} (figure 7*a*) causes almost simultaneous rollup of a larger leading vortex and a smaller trailing vortex while for a low AR_{xf}, the trailing vortex rolls up only after the leading vortex rolls up. On the other hand, for a fixed AR_{in}, a change in St_{θ_e} causes AR_{xf} to change because of the variations in the growth rate and saturation amplitude. Thus, by keeping AR_{in} fixed, one would expect differences in the strength, size, and distance between the rolled-up vortices due to changes in St_{θ_e}. Our measurements at fixed AR_{in} show that AR_{xf} increases with St_{θ_e} (figure 9*b*). The large increase in the AR_{xf} value for $St_{\theta_e} \geqslant 0.017$ is due to the larger growth rate of the subharmonic than the fundamental. Physically, vortices are produced at the subharmonic frequency, and the fundamental appears as the harmonic of the subharmonic. In the following, the effect of AR_{xf} on the proximity of vortices that eventually pair and the induction of the downstream paired vortices on the upstream pairing vortices are discussed. We consider two ranges of St_{θ_e} values: (i) $0.017 \leqslant St_{\theta_e} \leqslant 0.02$, for which $u'_{f/2}$ displays very little growth change near x_f, and (ii) $0.008 \leqslant St_{\theta_e} \leqslant 0.012$, for which $u'_{f/2}$ shows a significant decrease in the growth rate before it increases dramatically near x_f. Note that AR_{xf} is greater in case (i) than in case (ii). For these two cases, the configuration of vortices from flow visualization and their induced velocities are schematically shown in figure 9(*c*, *d*).

For case (i) (shown in figure 9*c*), the distance λ_1 between vortex 1 and vortex 2 is less than λ seen by visualization, the fundamental wavelength, while the distance between vortex 2 and the downstream paired vortex 3 is 2λ. As a result, the mutual induction between 1 and 2 (induced velocities are denoted as u_{12} and u_{21}) is stronger than the opposing motion u_{23} induced by 3. Thus, vortices 1 and 2 start rotating around each other, producing an increased subharmonic growth rate until their pairing is complete.

In case (ii), since AR_{xf} is smaller (figure 9*d*), vortices 1 and 2 do not roll up as close

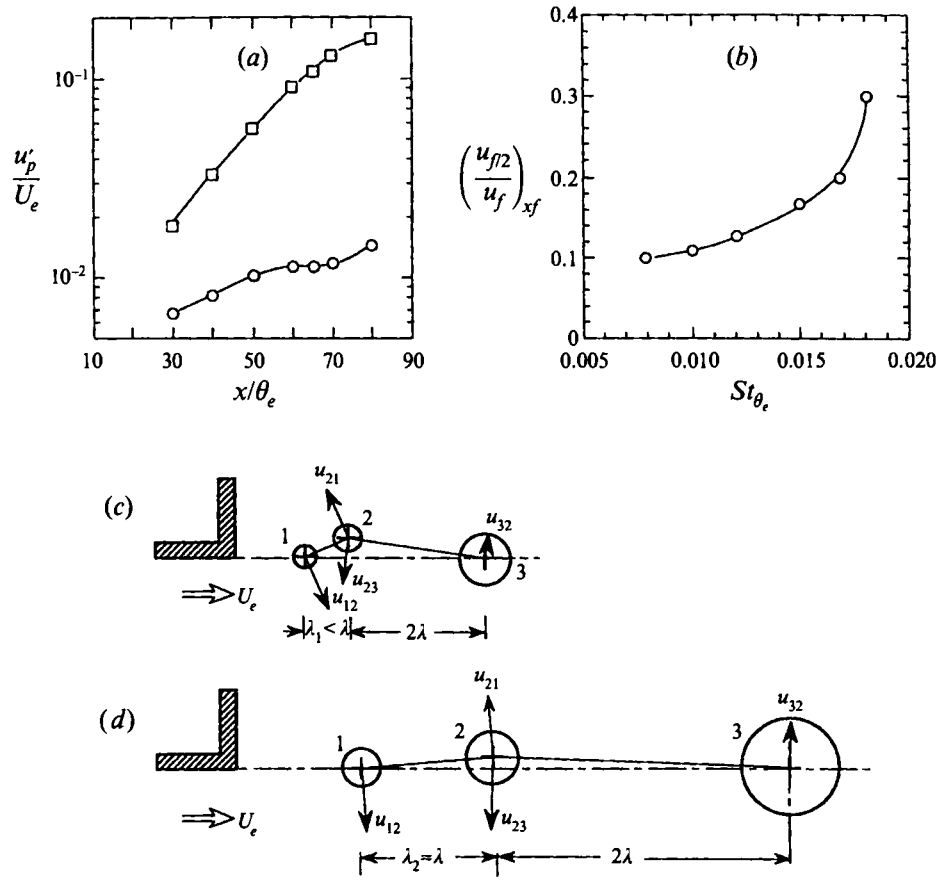

FIGURE 9. (*a*) Streamwise evolution of u'_f and $u'_{f/2}$ peaks at $St_{\theta_e} = 0.008$, showing zero growth rate of the subharmonic near $x_f \approx 60\theta_e$ for ϕ_{en}; □, u'_f; ○, $u'_{f/2}$. (*b*) Dependence of $AR_{xf} \equiv (u_{f/2}/u_f)_{xf}$ on St_{θ_e}. $a'_f = a'_{f/2} = 0.1\%$; $\phi = \phi_{en}$. (*c*, *d*) Schematics of vortex configuration and induced motions for: (*c*) high Strouhal number ($St_{\theta_e} \approx 0.017$); (*d*) low Strouhal number ($St_{\theta_e} \approx 0.008$).

to each other as in case (i). The distance between vortex 1 and vortex 2 is denoted as λ_2. Since vortex 1 begins to roll up after rollup of vortex 2 is nearly complete, u_{23}, induced by the paired vortex 3, pushes 2 down toward the lip line and thereby arrests the subharmonic growth over a short distance near x_f. However, as soon as vortex 1 rolls up, u_{21} increases and eventually supersedes u_{23}; this is because u_{12} and u_{13} (not shown) push it down so that vortex 1 gets closer to vortex 2. Thus vortices 1 and 2 begin pairing, producing an increased subharmonic growth rate.

Note that without a subharmonic, the circulation Γ of a vortex and the wavelength λ are both inversely proportional to St_{θ_e}, and hence the motion induced ($\sim \Gamma/\lambda$) on a vortex by its neighbour is independent of St_{θ_e}. However, in the presence of a subharmonic, visualization shows that decreased St_{θ_e} (and hence AR_{xf}) increases the dimensionless distance between pairing vortices, i.e. $\lambda_1/2\lambda < \lambda_2/2\lambda$. As a result, the net induction on vortex 2 by the downstream paired vortex 3 increases, so that pairing is further delayed with decreasing St_{θ_e}.

The parallel, or even slightly non-parallel, approximation does not allow vortex pairing through leapfrog motion (see figure 16 of Monkewitz 1988). Such an analysis

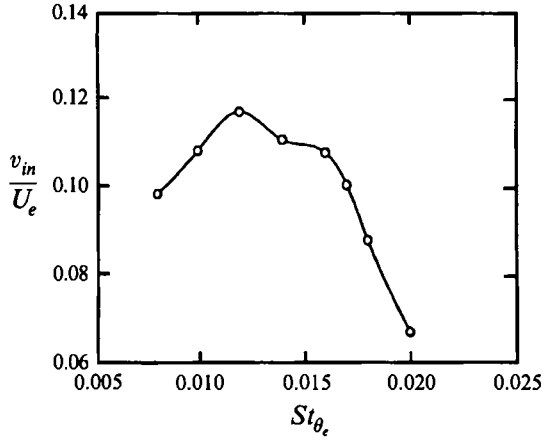

FIGURE 10. Dependence of the estimated induced velocity (v_{in}/U_e) at the lip on St_{θ_e}, caused by a rolled-up vortex, showing maximum v_{in}/U_e at $St_{\theta_e} \approx 0.012$.

cannot predict the subharmonic up to its saturation (i.e. completion of the pairing through leapfrogging) or, in turn, the decrease in the observed subharmonic amplitude for ϕ_{en} near x_f.

3.2.3. *Natural instability frequency and feedback*

Extending our analysis of vortex-induced motion, we now discuss the rollup frequency in naturally evolving shear layers. As previously noted, initially laminar shear layers were found to roll up at $St_{\theta_e} \approx 0.012$ (Zaman & Hussain 1980) while the theoretical value of the most unstable Strouhal number is $St_{\theta_e} \approx 0.017$. This experimental observation is believed to be a consequence of the feedback (caused by the induced velocity of rolled-up vortices) being strongest at $St_{\theta_e} \approx 0.012$ (Hussain 1986). From our experimental data we now estimate the feedback at various St_{θ_e}.

If we assume that the boundary-layer vorticity is advected at a velocity $U_e/2$ and rolls up into vortices at a frequency f, the circulation Γ per vortex is $U_e^2/2f\,(\equiv U_e\lambda)$. The leading-order term of the induced velocity v_{in} at the exit plane due to a rolled-up vortex at x_f is

$$v_{in} = \frac{1}{2\pi}\frac{\Gamma}{x_f} = \frac{1}{2\pi}\frac{U_e^2}{2f}\frac{1}{x_f},$$

and

$$\frac{v_{in}}{U_e} = \left[4\pi\, St_{\theta_e}\frac{x_f}{\theta_e}\right]^{-1}.$$

Induced velocities v_{in}/U_e (computed from x_f data) as a function of St_{θ_e} (figure 10) show that v_{in}/U_e reaches its maximum at $St_{\theta_e} \approx 0.012$, thus explaining the experimental observation of vortex rollup at $St_{\theta_e} \approx 0.012$.

Note that these are estimates of v_{in}/U_e, the total induced velocity. What is important for instability is the fluctuating part of the induced velocity at the lip from advecting vortices. An estimate using a row of advecting point vortices of equal strength and spacing shows that the resultant induced velocity fluctuations at the lip are about an order of magnitude less than the total induced velocity estimated from a single vortex at x_f (shown in figure 10). Relative levels shown in figure 10 should remain approximately the same if we consider fluctuations only. Thus, for unexcited shear layers $St_{\theta_e} \approx 0.012$ will produce the strongest feedback at the lip and will be self-sustained; we term this frequency the 'natural instability frequency'.

3.3. *Further details of the fundamental and subharmonic growth and their phase evolution*

In this section, we examine the effects of ϕ_{en} and ϕ_{at} on (i) the downstream evolutions of u'_f and $u'_{f/2}$ (along the lip line), (ii) the transverse distributions of $U(y)$, $u'_f(y)$ and $u'_{f/2}(y)$, and (iii) the streamwise variations of phase differences and phase velocities. The results are compared with the theoretical predictions of critical fundamental amplitude and the phase velocities required for resonant interactions. This can form a database for modelling nonlinear interactions in a non-parallel shear layer. Here we show results for excitation at $St_{\theta_e} = 0.012$ and its subharmonic with $a'_f = a'_{f/2} = 0.1\,\%$.

3.3.1. *Growth of the fundamental and the subharmonic*

The streamwise evolution of $u'_f(x)$ (figure 11*a*) illustrates that its growth and saturation are independent of ϕ (i.e. ϕ_{en} or ϕ_{at}) up to x_f. The subharmonic grows exponentially up to $x/\theta_e \sim 20$ irrespective of ϕ_{in}. When excited at ϕ_{en}, the growth rate of $u'_{f/2}$ is decreased near x_f owing to the induced motion of the downstream vortices undergoing pairing (explained in §3.2.2). Downstream of x_f, $u'_{f/2}$ grows resonantly and saturates at $x/\theta_e \sim 125$, indicating completion of pairing.

For excitation at ϕ_{at}, $u'_{f/2}$ decays near x_f but grows again farther downstream. Monkewitz (1988) predicts a monotonic decay of $u'_{f/2}$ with x for this critical value of ϕ in parallel flows. In reality, ambient disturbances cause pairing to occur randomly in space and time (see §3.1.2). This has also been suggested by Monkewitz (1988). Intermittent pairings result in a lower, yet growing, r.m.s. subharmonic amplitude (about 20 dB at $x \approx 60\theta_e$ and 7 dB at $x \approx 120\theta_e$, less than that for ϕ_{en}).

Traces of $\tilde{u}$ show a strong subharmonic component for ϕ_{en} (figure 11*b*), indicating periodic pairing. On the other hand, the $\tilde{u}$-traces for ϕ_{at} (figure 11*c*) show that the subharmonic appears and disappears intermittently. Sections of the $\tilde{u}$-traces containing a strong subharmonic component are drawn as thick lines, while the dashed parts indicate insignificant subharmonic content. The intermittent appearance of the subharmonic implies intermittent initiation of pairing. We speculate that feedback from an occasional pairing alters ϕ_{in} and triggers additional pairings. However, this phase will change owing to jitter in the pairing location so that ϕ_{at} required for pairing suppression may occasionally be attained (reflected by the disappearance of $f/2$ in the $\tilde{u}$-trace).

3.3.2. *Distributions of $U(y)$, $u'_f(y)$ and $u'_{f/2}(y)$*

Modifications of $U(y)$, $u'_f(y)$ and $u'_{f/2}(y)$ profiles due to phase changes (from ϕ_{at} to ϕ_{en}) were documented at a few x/θ_e locations.

$U(y)$ profiles are quite similar up to x_f (i.e. $x/\theta_e = 60$) for both ϕ_{en} and ϕ_{at} (figure 12*a*, *b*). Farther downstream, the profiles broaden more when excited at ϕ_{en} than at ϕ_{at}. The momentum thickness θ variations with x are shown in figure 12(*c*). (θ is computed by integrating between the limits $0.05 \leqslant U/U_e \leqslant 0.95$.) Close to the exit plane, the shear layer shows almost no growth up to $x/\theta_e \approx 20$. (The absence of growth near the exit was also observed by Hussain & Zedan (1978) and Husain & Hussain (1979) in the same facility with a smaller diameter nozzle.) Near the rollup location (from $x/\theta_e \approx 40$) the shear layer starts growing, and θ is almost independent of ϕ_{en} or ϕ_{at} up to this location. For excitation at ϕ_{en}, θ increases rapidly downstream of x_f because of the immediate onset of vortex pairing. For ϕ_{at}, θ increases at a much lower rate (almost half) than that for ϕ_{en} because of delayed, intermittent pairings.

Profiles of $u'_f(y)$ (figure 13*a–d*) up to x_f are almost identical for ϕ_{en} and ϕ_{at}. Note

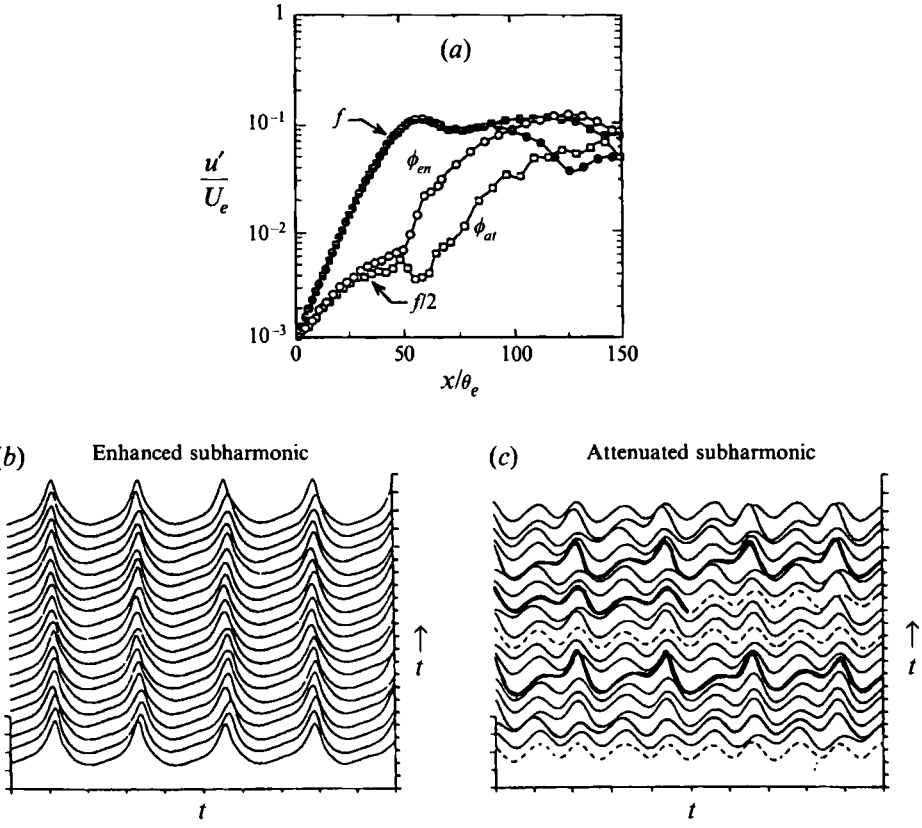

FIGURE 11. (*a*) Dependence of the growths of u'_f and $u'_{f/2}$ on ϕ_{en} and ϕ_{at}. $\oplus$, u'_f for ϕ_{en}; $\bigcirc$, $u'_{f/2}$ for ϕ_{en}; $\boxplus$, u'_f for ϕ_{at}; $\square$, $u'_{f/2}$ for ϕ_{at}. Note the early and delayed growth and saturation locations of $u'_{f/2}$. (*b*, *c*) Traces of u-fluctuations at $x/\theta_e = 125$ for: (*b*) ϕ_{en}; (*c*) ϕ_{at}. $St_{\theta_e} = 0.012$; $a'_f = a'_{f/2} = 0.1\,\%$. $U/U_c = 0.9$. Periodic pairings at the same location (periodic subharmonic in the velocity signal) occur for ϕ_{en}, while intermittent pairings (insignificant subharmonic shown by dashed line) occur for ϕ_{at}.

that the transverse location of the $u'_f(y)$ peak lies along the lip line up to x_f but shifts toward the high-speed side farther downstream. Distributions of $u'_{f/2}(y)$ in figure 14(*a–d*) show that, when excited at ϕ_{at}, the entire profile is suppressed significantly for $x/\theta_e \geqslant 30$ as expected owing to infrequent pairings. From the profiles for ϕ_{en}, the peak values of u'_f and $u'_{f/2}$ as a function of x are plotted in figure 15. The amplitude $u'_{f/2}(x)$ shows a decrease in its growth rate at $x/\theta_e \approx 35$ followed by an increase, at which point $u'_f/U_e \approx 0.03$. For $St_{\theta_e} = 0.017$ (not shown), the modified growth of $u'_{f/2}$ occurs at $u'_f/U_e \approx 0.04$. These values of u'_f/U_e are higher than the critical fundamental amplitude $u'_f/U_e = 0.015$ predicted by Monkewitz (1988) for a parallel shear layer. This difference appears to be due to the parallel-flow approximation in the theory. Contours of vorticity presented by Monkewitz (his figure 16) show that, even for slightly non-parallel flow, the two pairing vortices elongate in the streamwise direction and fuse together only in the region where they touch each other without rotating around each other. During this process, the peak vorticity is reduced to almost half that of the initial vortices. This elongated, diffuse vortex pair has less influence on the upstream vortices even at ϕ_{en} and therefore cannot cause an initial decrease in the subharmonic growth rate (before its resonant growth). (Although the vorticity distribution does not affect induced motion in the far field, it does in the near field.

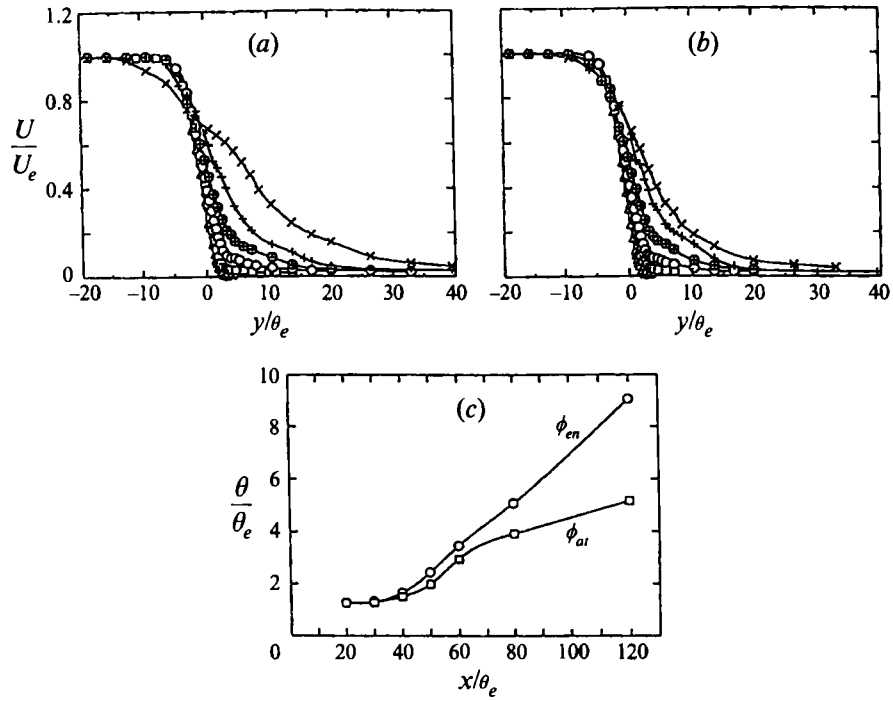

FIGURE 12. Profiles of $U(y)/U_e$ for: (*a*) ϕ_{en}; (*b*) ϕ_{at}. $St_{\theta_e} = 0.012$; $a'_f = a'_{f/2} = 0.1\,\%$. x/θ_e values are: △, 20; ◇, 30; □, 40; ○, 50; ⊕, 60; +, 80; ×, 120. (*c*) Streamwise variations of local momentum thickness θ/θ_e. ○, ϕ_{en}; □, ϕ_{at}. Note the increased spread for ϕ_{en}.

It appears that, for resonant interaction in a spatially evolving shear layer, the fundamental needs to grow to a level higher than the critical amplitude obtained by the parallel-flow approximation in order to counteract the influence of downstream pairing vortices. Our data also suggest that the critical fundamental amplitude depends on St_{θ_e}, as would be expected owing to the different strength and spacing of vortices at different St_{θ_e}.

3.3.3. *Phase velocity*

Phase velocities v_c were computed using the relations $\alpha_r = \partial\phi/\partial x$ and $v_c = \omega/\alpha_r$ where $\phi(x)$ is the phase of the wave at x and ω is the frequency (for details, see Hussain & Zaman 1978). Owing to large phase gradients of f and $f/2$ components across the shear layer, the uncertainty in phase velocity measurements can be large unless performed judiciously. We found the transverse location y where $U/U_e = 0.9$ to be suitable for phase measurements since the phase approaches an asymptotic value. As previously stated (in §3.1), phase measurements on the high-speed side provide more accurate data than on the low-speed side.

Streamwise variations of the fundamental and subharmonic phases and the local phase difference are shown in figure 16(*a–c*) for both ϕ_{en} and ϕ_{at}. The corresponding phase velocities are shown in figure 16(*d*, *e*).

Close to the exit, the local phases ϕ of f and $f/2$ (the phases ϕ of the fundamental and subharmonic waves are measured with respect to their own reference waves at the wave generator) show small changes with x (figure 16*a*, *b*), indicating large unrealistic phase velocities. (In particular, the subharmonic phase velocity up to $x/\theta_e \approx 15$ is

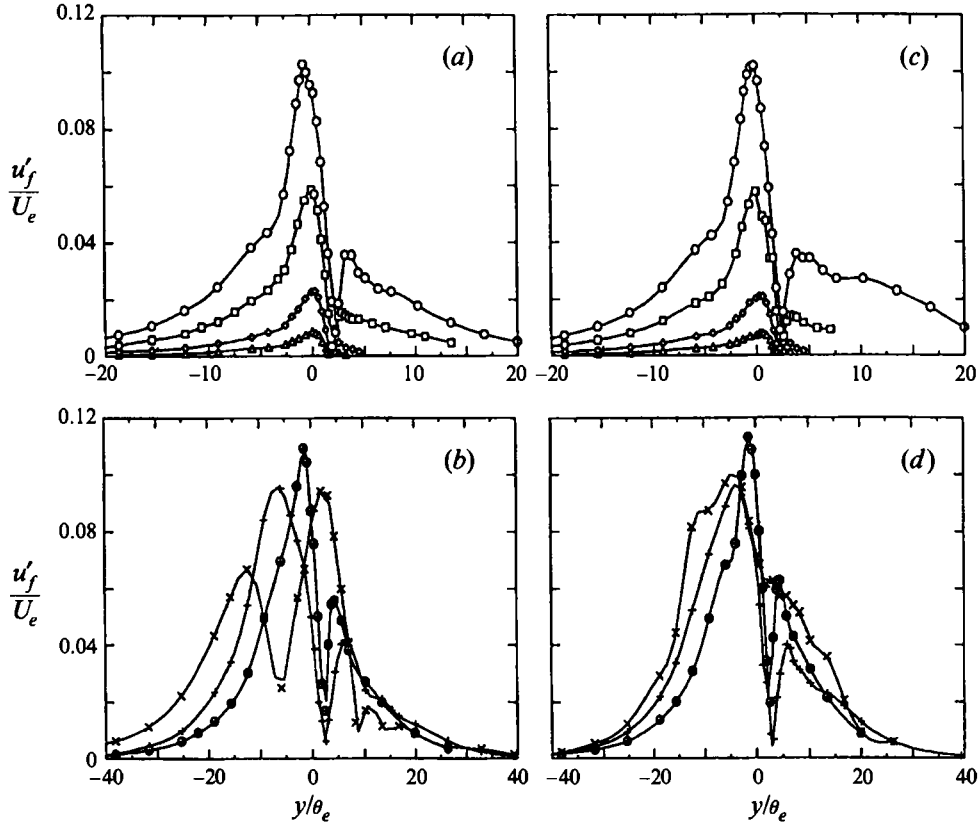

FIGURE 13. Profiles of $u'_f(y)/U_e$ for: (a, b) ϕ_{en}; (c, d) ϕ_{at}. $St_{\theta_e} = 0.012$, $a'_f = a'_{f/2} = 0.1\%$. Symbols are the same as in figure 12. There is no significant effect of ϕ_{tn} on $u'_f(y)$ up to $x \approx 60\theta_e$.

greater than the free-stream velocity U_e.) This is an artifact of the superposition of acoustic and hydrodynamic waves close to the shear layer origin (i.e. the excitation slit), where the contribution of acoustic waves presumably has dominant effects. (For details, see Rockwell & Schachenmann 1982.) For $20 \geqslant x/\theta_e \geqslant 40$ (figure 16*a*, *b*), lines indicate phase velocities of f ($v_c/U_e = 0.63$) and $f/2$ ($v_c/U_e = 0.83$) predicted by linear theory; in this range, theory agrees well with our data. Farther downstream, lines through the data show equal phase velocities ($v_c/U_e \approx 0.53$) of f and $f/2$).

Figure 16(*c*) shows that, for excitation at ϕ_{en}, the initial phase difference evolves from $\phi_{in} \approx 150°$ at the exit to 180° (equivalent to 0°; see (2.1)) near $x/\theta_e = 40$, and then decreases to 90° near x_f. Downstream of x_f, this phase difference remains constant (i.e. phase locks) as resonant $f/2$ growth occurs. For excitation at ϕ_{at}, the initial phase difference evolves from 72° to 180° near x_f, the critical value that suppresses $u_{f/2}$ growth. However, as discussed in §3.1, this critical value is difficult to maintain in a laboratory flow, and ambient disturbances will initiate occasional pairing. Note that Hajj *et al.*'s (1993) phase measurements along the u'_f peak line show $\phi_{xf} = 0°$ for maximum subharmonic enhancement, while we find this value to be $\pi/2$ on the high-speed side. This difference in the value of ϕ_{xf} is presumably an artifact of the transverse measurement location.

For both ϕ_{en} and ϕ_{at}, the subharmonic phase speed in the initial region is greater than that of the fundamental (figure 16*d*, *e*), which is consistent with the linear theory (Monkewitz & Huerre 1982). Local phase velocities are computed using third-order

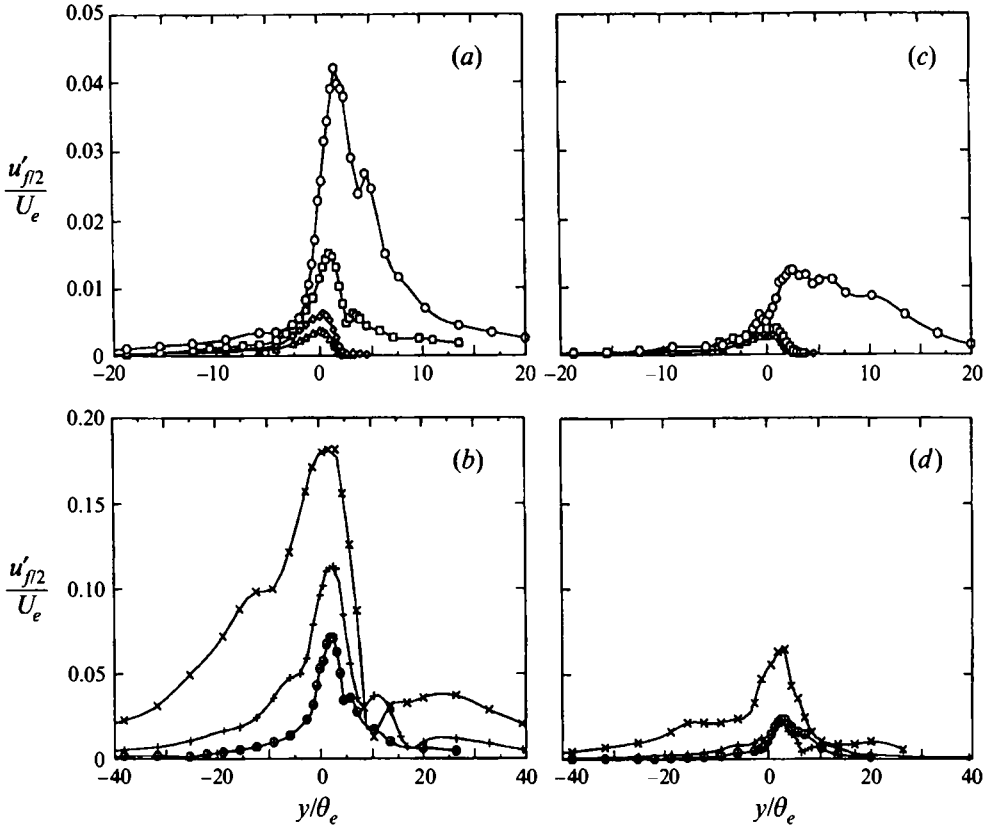

FIGURE 14. Profiles of $u'_{f/2}(y)/U_e$ for: (a,b) ϕ_{en}; (c,d) ϕ_{at}. $St_{\theta_e} = 0.012$, $a'_f = a'_{f/2} = 0.1\,\%$. Symbols are the same as in figure 12. Note the significant suppression of $u'_{f/2}(y)$ for ϕ_{at}.

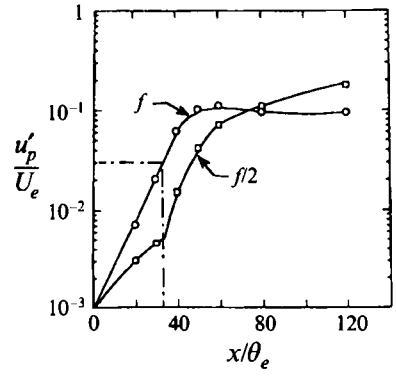

FIGURE 15. Streamwise variation of peak values of $u'_f(y)$ and $u'_{f/2}(y)$. $St_{\theta_e} = 0.012$, $\phi = \phi_{en}$, $a'_f = a'_{f/2} = 0.1\,\%$. ○, u'_f; □, $u'_{f/2}$. Critical fundamental amplitude u'_{fcr}/U_e (≈ 0.03), for which $u'_{f/2}$ experiences a modified growth rate, is denoted by the chain line.

polynomial fits to five adjacent data points. Note that two conditions need to be satisfied for resonance: (i) optimum phase difference between f and $f/2$ near x_f, and (ii) equality of phase speeds. For both ϕ_{en} (figure 16b) and ϕ_{at} (figure 16c), the fundamental phase speed v_c/U_e reaches a constant value of about 0.53 within a short

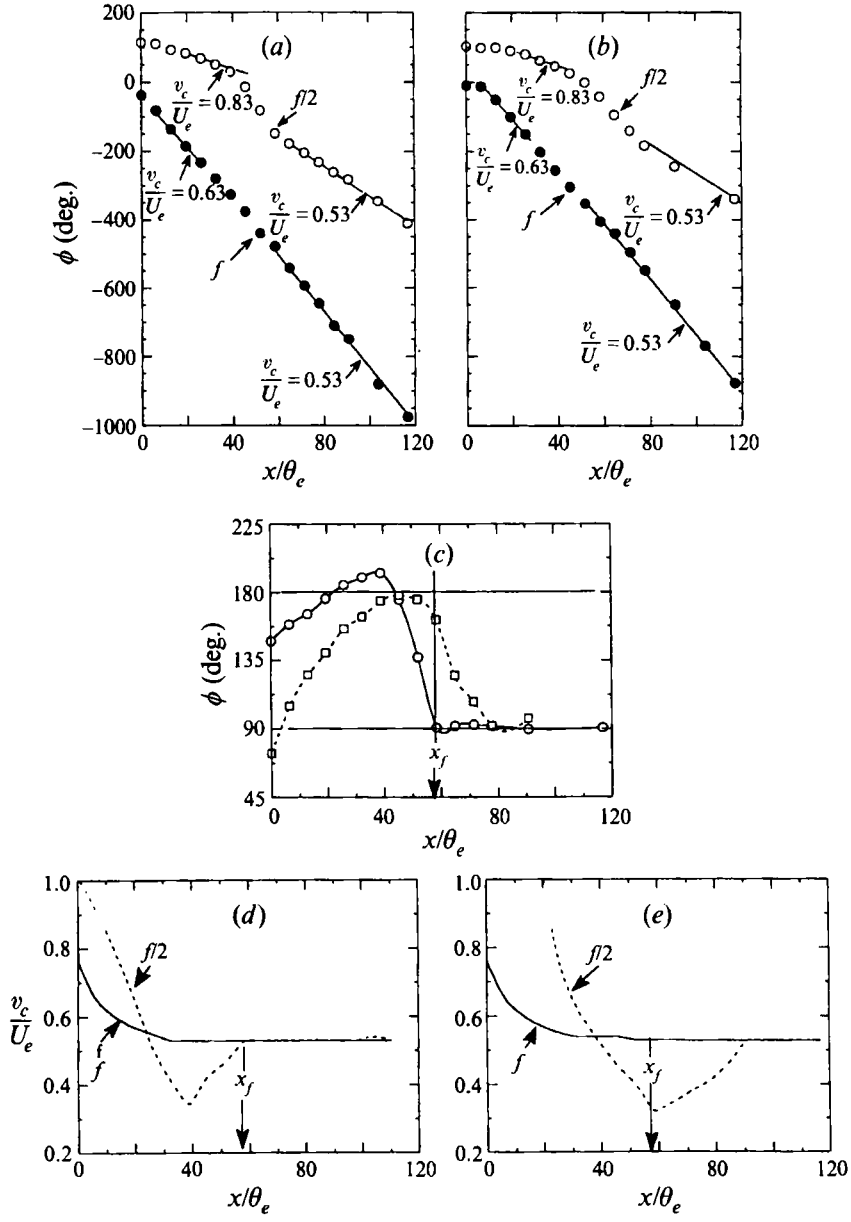

FIGURE 16. (*a*, *b*) Streamwise variations of local phase of f (●) and $f/2$ (○) for (*a*) ϕ_{en}; (*b*) ϕ_{en}. (*c*) Streamwise variations of local phase difference ϕ between f and $f/2$; ○, ϕ_{en}; □, ϕ_{at}. (*d*) Phase speed variations for ϕ_{en}; (*e*) phase speed variation for ϕ_{at}: ——, fundamental; – – –, subharmonic. $St_{\theta_e} = 0.012$; $a'_f = a'_{f/2} = 0.1\%$.

distance ($x/\theta_e \approx 30$, much before x_f) while the subharmonic phase speed rapidly decreases and reaches a value lower than that of the fundamental, then increases and eventually matches the fundamental phase speed. For ϕ_{at}, not unexpectedly, the phase speed of $f/2$ is matched farther downstream than for ϕ_{en}.

We have thus examined the roles of ϕ_{in} in the amplitude and phase evolutions of f and $f/2$. Furthermore, we have compared our results with theoretical predictions and found some agreements and some discrepancies which we have attempted to explain.

3.4. *Effects of detuning*

Unforced pairings do not occur periodically. In fact, spatial and temporal jitter in pairing is common even when rollup is forced periodically (and thus pairing is initiated by feedback or ambient disturbances), except for a limited range of St_{θ_e} and a'_f. This jitter is due to the inability of the subharmonic to phase lock; i.e. ϕ_{in} (due to f forcing and $f/2$ feedback) does not remain the same from one pairing to the next. When ϕ_{in} varies, so does the modified subharmonic growth rate and hence the pairing location. Aperiodic pairing typically occurs in an unforced flow owing to unlocked $f/2$ feedback phase (causing continuously changing ϕ_{in}). In order to explore this effect, we consider the simple case of linearly time-varying $\phi_{in}(t)$ via controlled detuned excitation. We therefore use detuned excitation to study the streamwise development of the sidebands as well as the subharmonic and to examine the mechanisms of phase and amplitude modulations in terms of vortex interactions.

To achieve detuned excitation, we employ two frequencies, either f and $f/2+\Delta f$ or f and $f/2-\Delta f$. (For the remaining discussion, we will denote such a forcing as f and $f/2\pm\Delta f$.) The introduction of $\pm\Delta f$ to the $f/2$ component is equivalent to a ϕ_{in} varying linearly with time, i.e.

$$u_{f/2+\Delta f} = B\cos[\pi ft+\phi_{in}(t)], \quad \text{where} \quad \phi_{in}(t) = 2\pi\Delta ft. \tag{3.1}$$

The experiments were performed at $St_{\theta_e} = 0.012$ and $a'_f = a'_{f/2\pm\Delta f} = 0.1\%$ for various values of Δf ($\Delta f/f = 0.5\%$, 2.5%, and 5%). For convenience, we denote the dominant lower and upper sidebands ($f/2-\Delta f$) and ($f/2+\Delta f$) by f_l and f_h respectively.

For a detuning of $\Delta f/f = 2.5\%$, the $\tilde{u}$-signal at $x/\theta_e = 120$ (figure 17*a*) shows modulations of the subharmonic phase and amplitude. The generation of multiple sideband frequencies $f/2\pm n\Delta f$ ($n = 1, 3, 5, \ldots$) is clear in the u-spectrum (figure 17*b*). A higher spectral resolution (figure 17*c*) shows the generation of $f/2\pm k\Delta f$ ($k = 0, 2, 4, \ldots$) sidebands also. Note that, unlike figure 17(*c*), figure 17(*b*) is a log-linear plot. These figures show that the amplitudes of $f/2\pm k\Delta f$ are much smaller than those of the neighbouring sidebands $f/2\pm n\Delta f$ and thus are not clear in figure 17(*b*).

An analysis (G. Broze 1995, private communication) using detuned coupled Landau-type equations for amplitude and phase shows that the linearly varying phase becomes sinusoidally varying when subharmonic resonance becomes important near the fundamental saturation, i.e. detuned excitation causes phase modulation when the evolution of the excited sideband becomes nonlinear. Furthermore, since phase changes affect the subharmonic growth rate and hence its amplitude at a fixed location upstream of pairing, detuned excitation also produces amplitude modulation with the same modulation frequency as that of the phase modulation (see Kim, Khadra & Powers 1980). Thus, we can consider a simple case where the phase and amplitude modulations are represented by cosine waves as

$$\begin{aligned} u(t) &= B_0(1+\mu\cos 2\pi f_m t)\cos(2\pi f_c t+\beta\cos 2\pi f_m t), \\ &= B_0(1+\mu\cos 2\pi f_m t)\sum_{n=-\infty}^{\infty} J_n(\beta)\cos(2\pi(f_c+nf_m)t), \end{aligned} \tag{3.2}$$

where μ is the amplitude modulation index, f_c is the carrier frequency (in the present case $f_c = f/2+\Delta f$), f_m is the modulation frequency for both amplitude and phase, β is the phase modulation index, and J_n is the Bessel function of the first kind of order n. (For more details on amplitude and phase modulations, see Roden 1991, pp. 153–249.) Note that, in each consecutive cycle of $f/2$, ϕ_{in} is advanced by $2\pi\Delta f$ radians. Therefore,

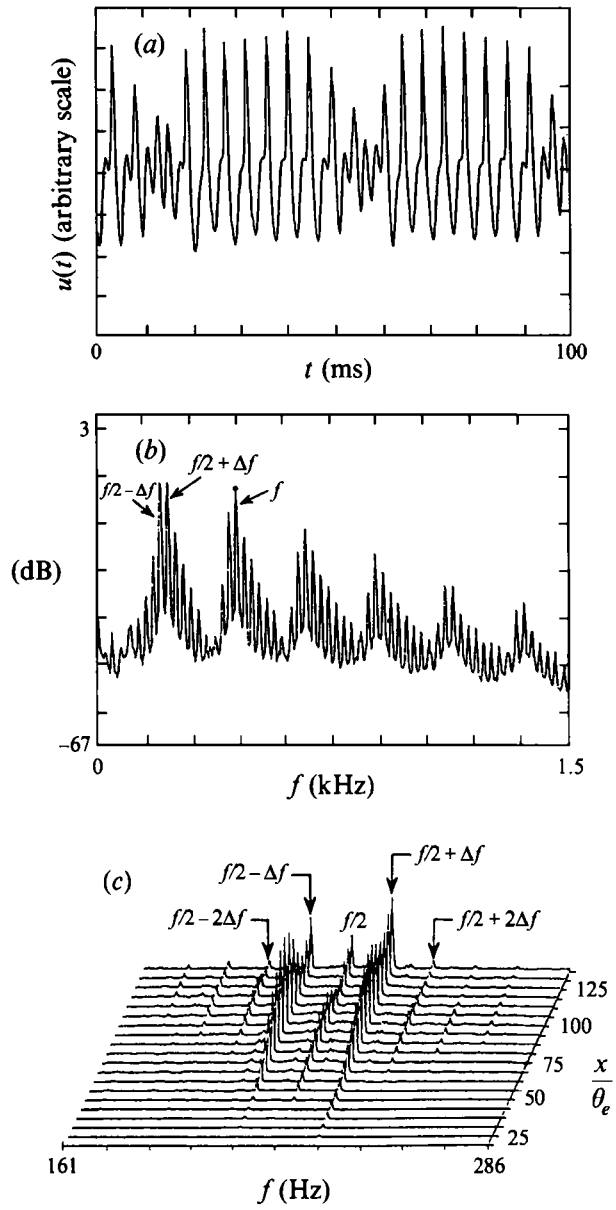

FIGURE 17. (*a*) $\tilde{u}$-trace and (*b*, *c*) power spectrum of u under detuned excitation, showing phase and amplitude modulations in the time trace and generation of sidebands in the spectra. $St_{\theta_e} = 0.012$; $\Delta f/f = 2.5\%$. $a'_f = a'_{(f/2+\Delta f)} = 0.1\%$.

to advance ϕ_{in} by π radians, the modulation period $T_m = \pi/2\pi\Delta f$. In other words, the modulation frequency is $f_m = 1/T_m = 2\Delta f$. The modulated signal in (3.2) contains all frequencies of the form $f_c + nf_m$ for $n = 0, \pm 1, \pm 2, \ldots$. Since f_c is the excited sideband (for instance $f/2 + \Delta f$ and $f_m = 2\Delta f$), such a modulation produces only the odd sideband frequencies (e.g. $f/2 + (1 + 2n)\Delta f$) and not the even sidebands (e.g. $f/2 + 2n\Delta f$) as observed in the velocity spectrum (figure 17*c*). The only way $f/2$ and its even sidebands can appear is through the generation of a modulation frequency Δf. This Δf then interacts with the odd sidebands to produce even sidebands. A spectral analysis of the amplitude and phase obtained from complex demodulation of a detuned

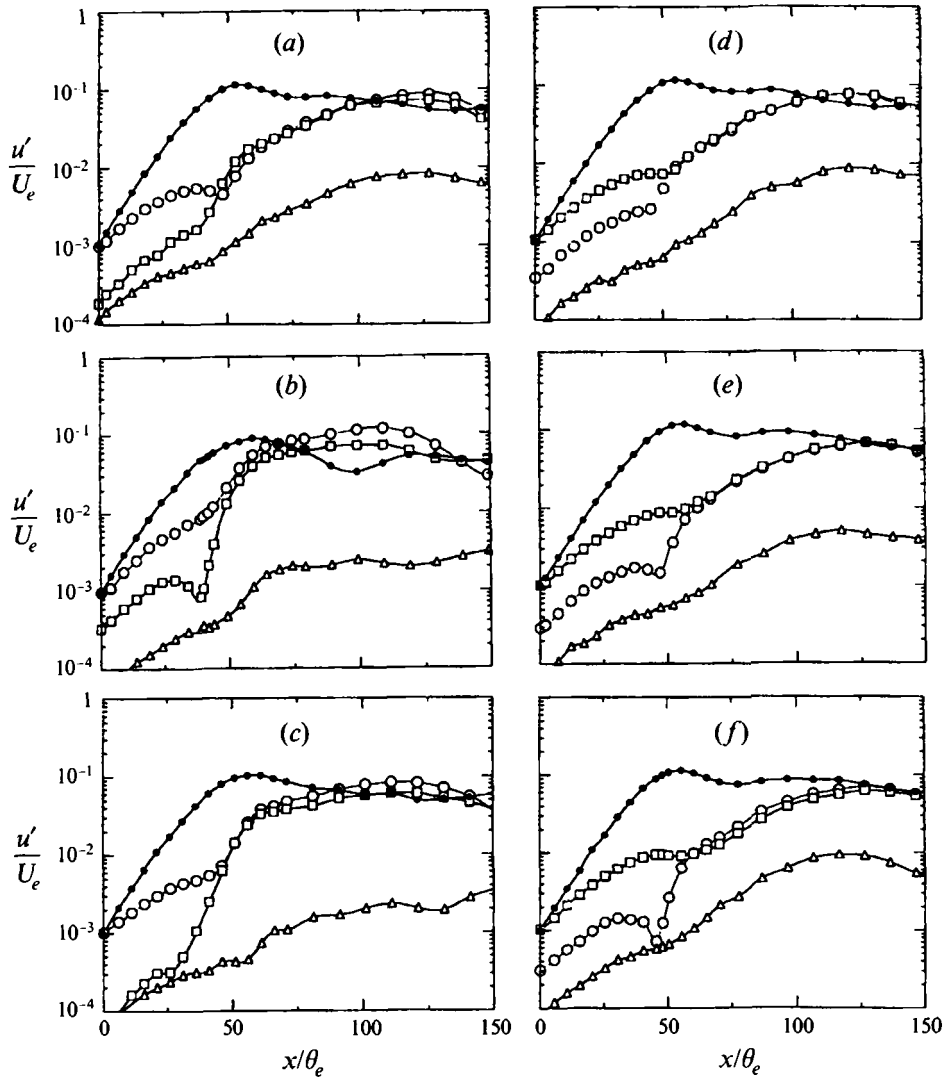

FIGURE 18. Growth of fundamental, subharmonic and two sidebands under excitation at various detuned frequencies. $St_{\theta_e} = 0.012$ and excitation levels are: $a'_f = a'_{(f/2-\Delta f)} = 0.1\%$ in (a,b,c); $a'_f = a'_{(f/2+\Delta f)} = 0.1\%$ in (d,e,f). Values of $\Delta f/f$ are: (a) -0.5%; (b) -2.5%; (c) -5%; (d) 0.5%; (e) 2.5%; (f) 5%. ●, u'_f; △, $u'_{f/2}$; □, $u'_{f/2+\Delta f}$; ○, $u'_{f/2-\Delta f}$. Note that the nonlinearly produced sideband grows at a high rate near x_f and reaches the level of the excited sideband.

velocity signal in a jet (G. Broze 1995, private communication) indeed reveals the presence of Δf, although at a much lower amplitude (about 20 dB below the level of $2\Delta f$). The mechanism of Δf generation is not clear, but its presence implies a timescale equivalent to two modulation wavepackets.

In figure 18$(a$–$f)$, the amplitude evolution of the two dominant sidebands f_l and f_h and the subharmonic $f/2$ along the shear layer lip line are shown for various values of Δf. When excited at f and a sideband, for instance f_h, the u'_f growth is essentially independent of Δf up to x_f. The r.m.s. amplitude of f_h (denoted by S_h) initially grows exponentially (up to $x/\theta_e \approx 20$) following linear theory, but near x_f it starts growing resonantly until its saturation near x_s. Simultaneously, the sideband f_l (produced via nonlinear interaction between f and f_h) starts growing, but at a much lower level.

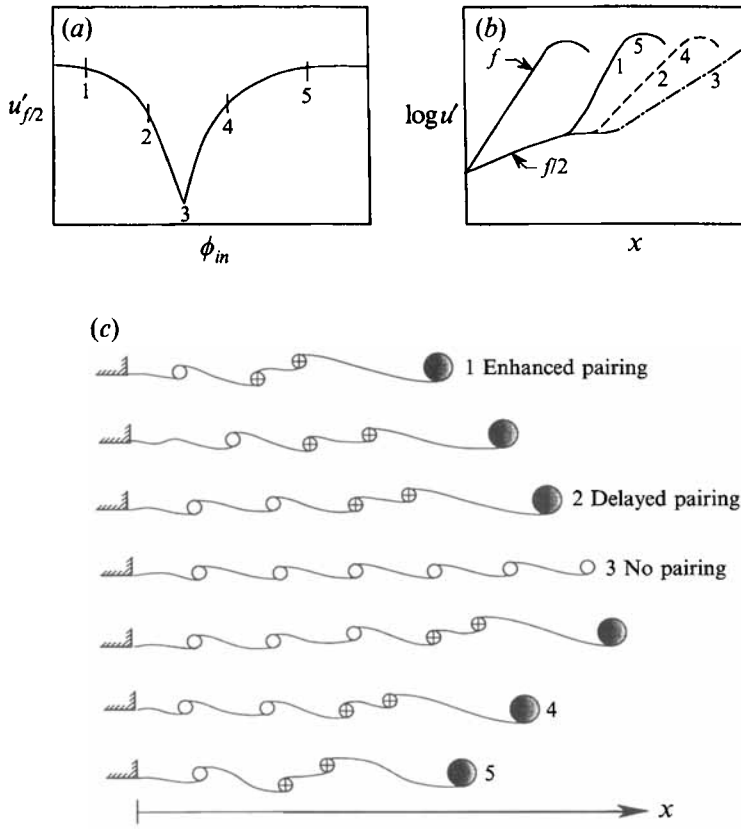

FIGURE 19. Schematics showing the effects of detuning on vortex pairing dynamics. (*a*) Dependence of $u'_{f/2}$ growth on ϕ_{in} at a given x-location downstream of x_f. (*b*) Dependence of the $u_{f/2}(x)$ growth rate modification on ϕ_{in}. (*c*) Corresponding vortex pairing configurations for various ϕ_{in}.

However, near x_f, its r.m.s. amplitude S_l starts growing at a much higher rate than S_h until its amplitude becomes comparable to S_h. Along with the two sidebands, the subharmonic amplitude also grows (but to a much lower level), changes its slope near x_f, and saturates farther downstream ($x/\theta_e > 100$). Several of our experimental results agree qualitatively with the analysis of Monkewitz (1988): (i) a higher growth rate of S_l then S_h near x_f and (ii) the symmetric growth (i.e. the same amplitudes and growth rates of S_h and S_l) and saturation of both sidebands farther downstream. Similar results are obtained for excitation at f and f_l. We find that the degree of detuning ($\Delta f/f \leqslant 5\%$) we used has very little effect on the growth patterns of S_h and S_l.

We now examine the effects of detuned excitation in terms of vortex pairing. In the region between x_f and x_s, flow visualization reveals that the pairing location moved upstream and downstream nearly periodically because of changing ϕ_{in}. The suppression phase ϕ_{at} occurs at most once in each modulation cycle, and hence occasionally one vortex escapes pairing in each cycle. The shift in the pairing location due to phase variation at the exit plane caused by detuning is shown schematically in figure 19. Figure 19(*a*) shows qualitatively the dependence of $u'_{f/2}$ on ϕ_{in} (similar to figure 3). In this figure, five arbitrary phases are chosen: one (3) at the maximum attenuation phase, two (1 and 5) near the maximum enhancement phases, and two (2 and 4) phases in between. The corresponding delayed, modified growths of the subharmonic are shown qualitatively in figure 19(*b*). Note that as ϕ_{in} passes through

phases 1 to 5 and back to 1, the $u'_{f/2}$ growth rate decreases and then increases, and so its saturation location moves downstream and upstream. The corresponding vortex configurations and the shift in the vortex pairing location are sketched in figure 19(*c*).

As previously stated, we expect similar pairing dynamics to occur with single-frequency excitation or even without forcing since, in general, the uncontrolled $f/2$ perturbation at the receptivity point due to feedback from pairing is naturally detuned. Thus phase-locking of $f/2$ may not occur and pairing will not be periodic. In this situation, the flow may reveal low-dimensional dynamics. In fact, studies of jets (Broze & Hussain 1994) and shear layers (Narayanan & Hussain 1995) using single-frequency forcing found self-detuned pairings and double pairings associated with low-dimensional chaos.

We emphasize that the generation of sidebands occurs even for laminar well-defined vortices. Spectral broadening around $f/2$ in a natural shear layer at a location downstream of x_f does not necessarily imply transition to turbulence, as is often inferred (e.g. see Miksad *et al.* 1982; Thomas 1990). The spectral broadening is due to random phase jitter between f and $f/2$, causing the pairing location to move randomly in space and does not necessarily reflect breakdown of large-scale vortices (i.e. mixing transition).

4. Concluding remarks

While linear theory predicts quite accurately the initial development, a wave description for nonlinearities in a diverging flow, including vortex interactions, is a challenging task, even under the assumptions of weakly nonlinear and slightly non-parallel flows. It seems quite natural to explore the subharmonic resonance phenomenon in terms of vortex dynamics as was done here.

Controlled two-frequency excitation (both tuned and detuned) has allowed us to examine systematically the roles of ϕ_{xf} and AR_{xf} in altering vortex configurations (e.g. strengths and streamwise and transverse displacements) and subsequent vortex interactions. Pairing is stabilized over a wide range of ϕ_{xf}, while attenuation of the subharmonic, i.e. non-pairing vortex advection, occurs at a critical value of ϕ_{xf}. In laboratory flows, however, such an unstable configuration of vortices cannot persist because disturbances (ambient as well as pairing feedback) initiate vortex pairing randomly. We have identified a wide St_{θ_e} range over which pairing can be controlled (enhanced or suppressed) with low-level, two-frequency excitation.

We differentiate shredding from either non-pairing or complete pairing of vortices. Shredding can be considered to be a fractional pairing process (observed experimentally) where a strong vortex captures parts of a neighbouring weak vortex. From velocity signals, it is difficult to differentiate unambiguously between shredding and enhanced pairing.

By detuning we have studied the evolution of natural (unexcited) and excited (single-frequency) shear layers. In the case of single-frequency excitation, subharmonic perturbations at the origin appear owing to feedback from vortex pairings. Periodic pairing occurs if ϕ_{in} between subharmonic (from feedback) and the excited fundamental falls in the range which initiates pairing (i.e. ϕ_{en}) and remains the same in each pairing cycle. This phase locking is found to occur under single-frequency excitation at $St_{\theta_e} \approx 0.012$ at low excitation levels. On the other hand, when excited near $St_{\theta_e} = 0.017$ (for similar amplitudes as those required for periodic pairing at $St_{\theta_e} \approx 0.012$), the appearance of a weak subharmonic (Zaman & Hussain 1981) suggests that the feedback is not locked and remains close to ϕ_{at} most of the time,

causing suppressed or delayed pairings. In natural jet and shear layers, although fundamental excitation can occur owing to some facility-dependent resonance, periodic pairings are rare and detuning is common. Because of random jitter in the pairing location, the velocity spectrum shows a broad band instead of sharp sideband peaks. Such spectral broadening involves sideband instabilities resulting from random phase jitter and does not necessarily indicate transition to turbulence.

The authors are grateful to Dr George Broze and Mr Satish Narayanan for fruitful discussions and careful reviews of the manuscript and to Mr Bill Berger for making some of the figures. We acknowledge fruitful discussions with Professor Peter Monkewitz during early stages of this study. This work was supported by the Office of Naval Research grant N00014-89-J-3231, Air Force Office of Scientific Research grant F49620-92-J-0200, and Texas ARP grant 003652-151.

REFERENCES

ANDERSON, A. B. C. 1955 *J. Acoust. Soc. Am.* **27**, 1048.

ARBEY, H. & FFOWCS WILLIAMS, J. E. 1984 *J. Fluid Mech.* **149**, 445.

BALSA, T. F. 1987 *J. Fluid Mech.* **174**, 553.

BRADSHAW, P. 1966 *J. Fluid Mech.* **26**, 225.

BRIDGES, J. & HUSSAIN, F. 1987 *J. Sound Vib.* **117**, 289.

BROWAND, F. K. 1966 *J. Fluid Mech.* **26**, 281.

BROZE, G. & HUSSAIN, F. 1994 *J. Fluid Mech.* **263**, 93.

CHENG, M. & CHANG, H. 1992 *Phys. Fluids* A **4**, 505.

CORCOS, G. M. & SHERMAN, F. S. 1984 *J. Fluid Mech.* **139**, 29.

DRUBKA, R. E. 1981 Instability in near field of turbulent jets and their dependence on initial conditions and Reynolds number. PhD dissertation, Illinois Institute of Technology.

FREYMUTH, P. 1966 *J. Fluid Mech.* **25**, 683.

GOLDSTEIN, M. E. & LEIB, S. J. 1988 *J. Fluid Mech.* **191**, 481.

HAJJ, M. R., MIKSAD, R. W. & POWERS, E. J. 1993 *J. Fluid Mech.* **256**, 404.

HO, C. M. & HUANG, L. S. 1982 *J. Fluid Mech.* **119**, 443.

HO, C. M. & HUERRE, P. 1984 *Ann. Rev. Fluid Mech.* **16**, 365.

HULTGREN, L. S. 1992 *J. Fluid Mech.* **236**, 635.

HUSAIN, Z. D. & HUSSAIN, A. K. M. F. 1979 *AIAA J.* **17**, 48.

HUSSAIN, A. K. M. F. 1983 *Phys. Fluids* **26**, 2816.

HUSSAIN, A. K. M. F. 1986 *J. Fluid Mech.* **173**, 303.

HUSSAIN, A. K. M. F. & CLARK, A. R. 1977 *Phys. Fluids* **20**, 1416.

HUSSAIN, A. K. M. F. & ZAMAN, K. B. M. Q. 1978 *J. Fluid Mech.* **87**, 349.

HUSSAIN, A. K. M. F. & ZEDAN, M. E. 1978 *Phys. Fluids* **21**, 1475.

KELLY, R. E. 1967 *J. Fluid Mech.* **27**, 657.

KIM, Y. C., KHADRA, L. C. & POWERS, E. J. 1980 *Phys. Fluids* **23**, 2250.

LAUFER, J. 1974 *Omaggio Carlo Ferrari*, p. 451. Libreria Editrice Universitaria Lerrotto & Bella, Torio.

MANKBADI, R. R. 1985 *J. Fluid Mech.* **160**, 385.

MICHALKE, A. 1965 *J. Fluid Mech.* **23**, 521.

MIKSAD, R. W., JONES, F. L., POWERS, E. J., KIM, Y. C. & KHADRA, L. 1982 *J. Fluid Mech.* **123**, 1.

MONKEWITZ, P. A. 1988 *J. Fluid Mech.* **188**, 223.

MONKEWITZ, P. A. & HUERRE, P. 1982 *Phys. Fluids* **25**, 1137.

NARAYANAN, S. & HUSSAIN, F. 1995 Measurements of spatiotemporal dynamics in a forced plane mixing layer. (Submitted.)

PASCHEREIT, C. O., WYGNANSKI, I. & FIEDLER, H. E. 1995 *J. Fluid Mech.* **283**, 365.

PIERREHUMBERT, R. T. & WIDNALL, S. E. 1981 *J. Fluid Mech.* **102**, 301.
PIERREHUMBERT, R. T. & WIDNALL, S. E. 1982 *J. Fluid Mech.* **114**, 59.
RILEY, J. J. & METCALFE, R. W. 1980 *AIAA Paper* 80-0274.
ROCKWELL, D. & SCHACHENMANN, A. 1982 *J. Fluid Mech.* **117**, 425.
RODEN, M. S. 1991 *Analog and Digital Communication Systems.* Prentice Hall.
SATO, H. 1959 *J. Phys. Soc. Japan* **14**, 1797.
STUART, J. T. 1967 *J. Fluid Mech.* **29**, 417.
THOMAS, F. O. 1990 *Phys. Fluids* A **2**, 553.
ZAMAN, K. B. M. Q. & HUSSAIN, A. K. M. F. 1980 *J. Fluid Mech.* **101**, 449.
ZAMAN, K. B. M. Q. & HUSSAIN, A. K. M. F. 1981 *J. Fluid Mech.* **103**, 113.